LEONARDO: Low Earth Orbit Novel Advanced Radiation Diurnal Observation

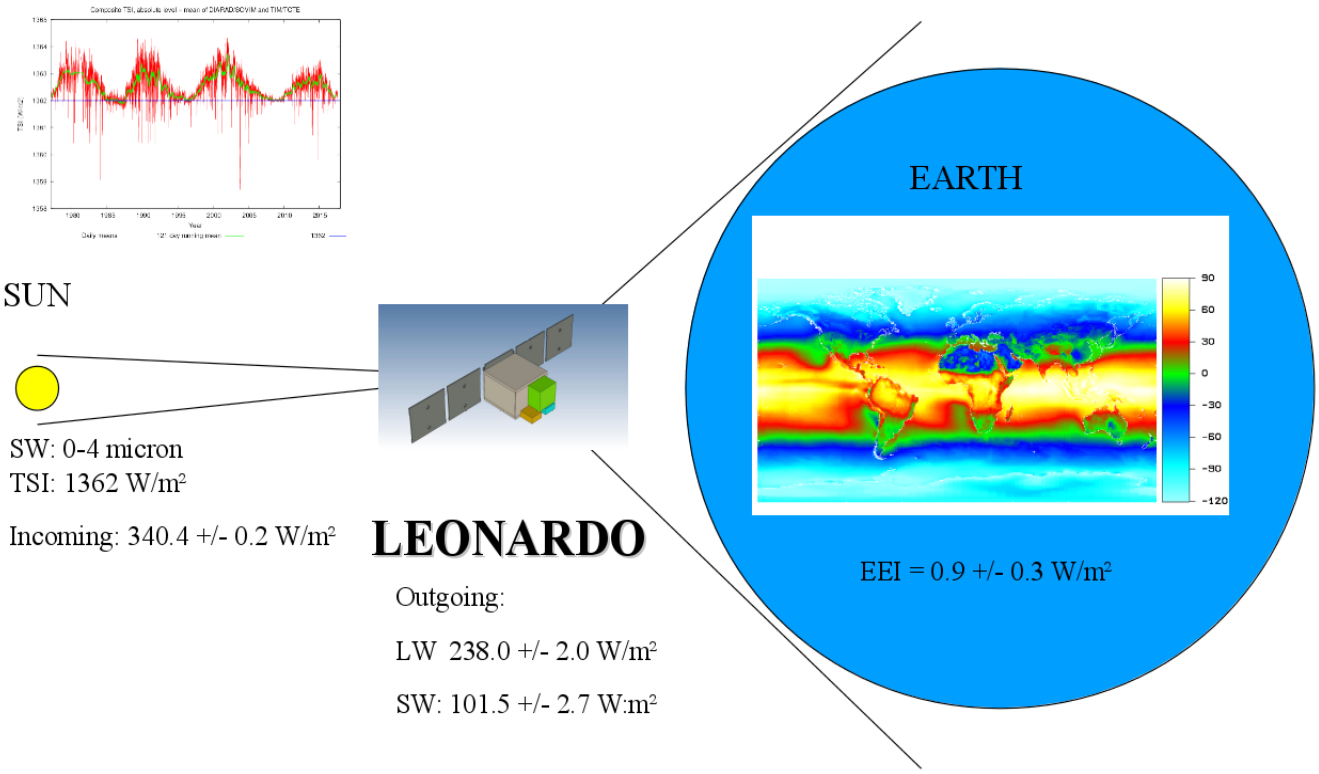

An ESA Earth Explorer-10 Mission Idea

Lead Proposer:

Dr. Steven Dewitte
Royal Meteorological Institute of Belgium
Ringlaan 3, 1180 Brussels, Belgium
+32-2-3730624
steven.dewitte@meteo.be

Proposing Team

Lead Proposer: Dr. Steven Dewitte – Royal Meteorological Institute of Belgium

Technical Team:

Frank Preud'homme – QinetiQ Space – Satellite provider
Chabely Pollier – QinetiQ Space – Satellite provider
Dr. Martin Caldwell – RAL Space – Broadband spectrometer instrument design
Dr. Holger Fritsch – Jena-Optronik – Wide field of view cameras instrument design
Prof. Francis Berghmans – VUB – Optical design
Prof. Michael Vervaeke – VUB – Optical design
Dr. Lien Smeesters – VUB – Optical design

Science Team:

Dr. Nicolas Clerbaux – Royal Meteorological Institute of Belgium – Earth Radiation Budget science.
Prof. Richard Allan – University of Reading - Earth Radiation Budget science.
Dr. Mustapha Meftah – LATMOS/CNRS – Solar science and instrument design
Dr. Stijn Nevens – Royal Meteorological Institute of Belgium – Total Solar Irradiance & cavity radiometer science.
Dr. Olivier Boucher – LMD – Aerosol and cloud science
Dr. Stefan Kinne – MPI Met - Aerosol and cloud science
Prof. Carmine Serio – University of Basilicata – Radiative transfer and atmospheric retrievals
Dr. Jan Fokke Meirink – KNMI - Clouds science

Table of Contents

1. Executive Summary

The Low Earth Orbit Novel Advanced Radiation Diurnal Observation (LEONARDO) mission idea aims at the **first ever significant direct radiative measurement of the Earth's Energy Imbalance (EEI) together with underlying variables such as clouds, aerosols, temperature and humidity**. This measurement is crucial for our **understanding of current climate change**, and our ability to **predict future climate change** [Hansen et al, 2011].

The Earth Radiation Budget (ERB) at the top of the atmosphere quantifies how the earth gains energy from the sun and loses energy to space. It is of fundamental importance for climate and climate change since

1) The global climate, as quantified e.g. by the global average temperature, is determined by this energy exchange.
2) The insolation is stronger at the equator than at the poles, the resulting net ERB at the equator is positive, while it is negative at the poles. The equator to pole gradient of the ERB is the driver of the general circulation in the atmosphere – hence of weather and climate - and the oceans, which transports heat from the equator to the poles.
3) In a climate in equilibrium the ERB terms are in balance. Climate change, as we are currently experiencing, is provoked by an ERB imbalance, also called Earth Energy Imbalance (EEI).

The current state of our knowledge of the ERB as reviewed in [Dewitte & Clerbaux, 2017] is illustrated in figure 1.

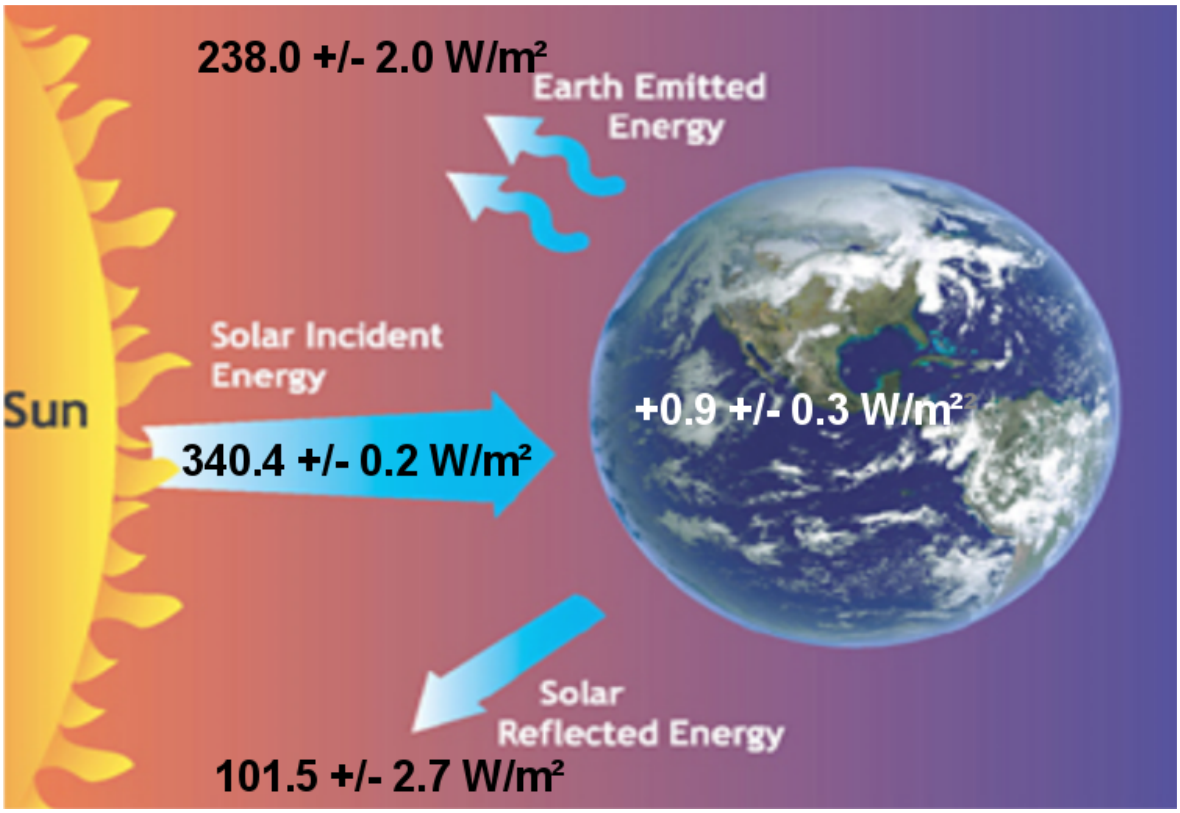

Figure 1: Earth Radiation Budget terms as reviewed in [Dewitte & Clerbaux, 2017].

In a climate in equilibrium the ERB is in balance and the EEI is zero. The primary causes of climate change are radiative forcings. Radiative forcings are externally imposed perturbations of the equilibrium ERB. Figure 2 illustrates the positive (heating) radiative forcing of GreenHouse Gases (GHG's), partially compensated by a negative (cooling) radiative forcing by aerosols according to [Hansen et al, 2011]. **The uncertainty on the net radiative forcing is dominated by the uncertainty on the aerosol forcing. The measurement of the EEI will allow to signifcantly reduce this uncertainty.**

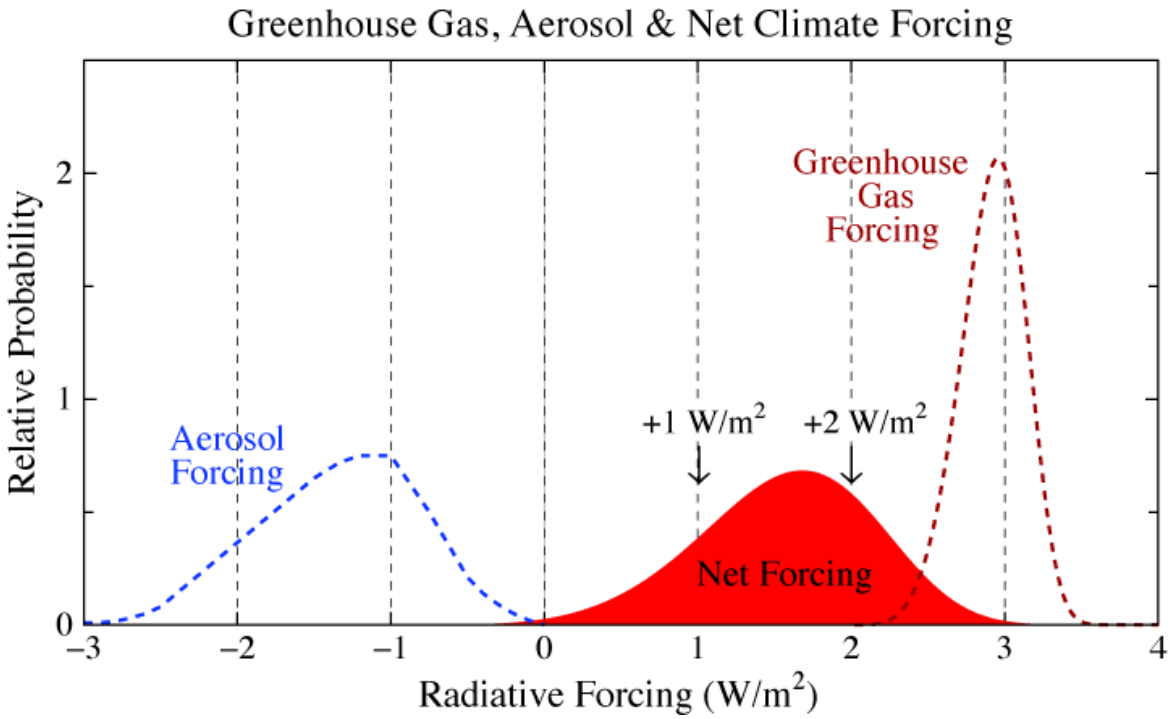

Figure 2: Reproduction of fig. 2 of [Hansen et al, 2011] illustrating the GHG, aerosol, and net radiative forcing and their uncertainties.

In response to a positive radiative forcing, the earth is heating in order to reach a new equilibirum temperature with increased emitted thermal radiation. This heating occurs with a delayed time response mainly due to the thermal inertia of the oceans. **The measurement of the EEI allows to directly assess the amount of "heating in the pipeline"**, i.e. the amount of heating that will occur before the new equilibrium temperature is reached [Hansen et al, 2011].

Despite its fundamental importance the **Earth Energy Imbalance (EEI)** remains challenging to measure directly through radiation measurements. It is the small difference between two nearly equal terms of opposite sign: the incoming solar radiation and the total earth leaving radiation. Up to now the two terms are measured with separate instruments, with independent calibration errors, which are added. The sum of the calibration errors overwhelms the small difference to be measured. We propose a breakthrough novel approach making measurements of the incoming solar radiation and the earth leaving radiation with exactly the same instrument, resulting in a **true differential measurement** of the EEI.

Besides the calibration, also the space-time sampling of the earth is challenging. With a classical Sun Synchronous Orbit (SSO), global coverage is obtained, but for all locations on earth except the polar regions, only two measurements per day are obtained. This provides insufficient sampling of the diurnal cycle. We propose to use an **inclined orbit at 80° inclination**, which combines global coverage with a slow precession, resulting in an **adequate statistical sampling of the diurnal cycle at the seasonal timescale** when used on a standalone base. Moreover, due to its slow precession, the Leonardo orbit will move in and out of phase with existing instruments on SSO orbits, such as in afternoon orbits CERES on NPP and NOAA-20, the CERES successor RBI on JPSS-2, and in the morning orbit AVHRR on Metop or METimage on Metop SG. This will allow intercalibration with these existing instruments, and the calibration of diurnal cycle models of these instruments in SSO orbits. The combination of Leonardo with the existing SSO instruments will provide an **adequate statistical sampling of the diurnal cycle at the monthly mean timescale**.

Scientific objectives

The scientific objectives of the Leonardo mission idea are

1) to make direct measurements of the annual mean EEI with an unprecedented accuracy of the order of 0.1 W/m².
2) to measure the Total Solar Irradiance - which determines the incoming solar radiation – with an absolute accuracy of 1 W/m².
3) to measure the outgoing ERB components of Reflected Solar Radiation (RSR) and Outgoing Longwave Radiation (OLR) with adequate statistical sampling of the monthly mean diurnal cycle, with global spatial sampling at a spatial resolution allowing the separation of cloudy and clear sky scenes.
4) to make joint measurements of the Aerosol Optical Depth (AOD), allowing to make an assessment of the direct aerosol radiative effect.
5) to make joint measurements of the main atmospheric and surface parameters that influence the ERB.

Characteristics of the mission

The Leonardo mission idea is to fly a combination of 3 passive optical instruments on a **single low earth orbit satellite with 80° inclination**. The scientific objectives will be reached in synergy with existing instruments on existing SSO orbits.

The unprecedented targeted accuracy for the EEI measurement depends critically on the measurement of the incoming solar and the outgoing terrestrial radiation with a single instrument. The core instrument - intended for this purpose - is a **Wide Field of View (WFOV) Electrical Substitution (ES) Cavity Radiometer (CR)**. In standard operation it will be pointed to earth, for intercalibration it will be pointed to the sun periodically, e.g. by reversing nadir and zenith pointing once every 83 days when the sun is in the orbital plane. Technical novelties in the proposed design of the CR are: 1) the use of **Vacuum Aligned Carbon NanoTubes (VACNT)** as black material, 2) a near spherical cavity shape design for a near uniform angular absorption of the cavity, 3) a dedicated baffle allowing an unvignetted field of view of 130°, 4) **spatially distributed electrical substitution** using heating resistors and temperature sensors at multiple locations, 5) the **in-flight use of the sun as a point source to characterise the spatial non-uniformity** of the CR.

The WFOV radiometer observes the earth from limb to limb. The spatial resolution of a WFOV measurement is of the order of 5900 km. In order to reach the spatial resolution at which cloud and clear sky scenes can be discriminated a resolution enhancement is needed. To this end auxiliary **WFOV hemispherical Shortwave (SW) and Longwave (LW) cameras** will be used. The cameras will consist of a fish eye lens in front of **uncooled** detector arrays. As a SW detector array a backlit CCD with spectral sensitivity in the range from 400 to 900 nm will be used. As a LW detector an uncooled microbolometer array with spectral sensitivity in the range from 8 to 14 micron will be used. As a baseline detector arrays with 1024x1024 pixels will be used, resulting in a nadir resolution of 3.9 km. The use of uncooled detectors is beneficial for power and mass efficiency and for instrument stability.

As third instrument **a combined SW and LW broadband imaging spectrometer** will be added for the characterisation of the main parameters influencing the ERB. This broadband spectrometer will use flight proven **gold black coated microbolometer detectors**, allowing broadband measurements from 0.3 to 100 micron. It will have a nadir resolurtion of 4.4 km. **Linear Variable Filters** will be used for innovative additional coarse resolution spectral measurements. 7 SW bands from 300 to 1700 nm and 8 LW bands from 6 to 14 micron will be used. This instrument will have heritage from the AVHRR instrument for the scan mirror concept, and from the Gerb and the Earthcare BBR instruments for the detectors and the calibration sources. It will use **an advanced freeform 6° x 6° field of view telescope**.

2. Scientific Objectives, Requirements and Justification

2.1 Mission objectives and rationale

The climate on earth is fundamentally described by the Earth Radiation Budget (ERB), which describes how the earth gains energy from the sun in the form of Total Solar Irradiance (TSI), and loses energy to space in the form of reflected solar radiation and emitted thermal radiation. The current state of our knowledge of the ERB is summarised in [Dewitte & Clerbaux, 2017].

For a climate in equilibrium the outgoing terms of the ERB are in balance with the incoming solar radiation. Any perturbation of an ERB term compared to this equilibirium state is called a radiative forcing, and is a driver for climate change. The most important radiative forcings are a positive (heating) forcing by greenhouse gases and a negative (cooling) forcing by aerosols.

Two key uncertainties limit our understanding of current climate change and our capacity of predicting future climate change [Hansen et al 2011]: 1) the uncertainty on the aerosol forcing is large and dominates the uncertainty on the net forcing , 2) the rate at which the earth's climate system reaches a new equilibrium is determined by the amount of mixing of heat perturbations into the deeper ocean,. This amount of ocean mixing is also uncertain. The joint observation of global temperature change and the Earth Energy Imbalance (EEI) allows to resolve the aerosol and ocean uncertainties – see figures 3 and 4 – and thus significantly increase our understanding of current climate change, and increase our ability to predict future climate change.

The Earth Energy Imbalance (EEI) is defined as the difference between the incoming solar and outgoing terrestrial ERB terms. It is the most fundamental climate change metric, and it should be monitored with an accuracy of 0.1 W/m² [Hansen et al, 2011] [Von Schuckmann et al, 2016]. It quantifies the amount of net forcing that the earth's climate system has not yet responded to. EEI and its changes will determine the future of earth's climate. It is thus imperative to measure EEI and the factors that are changing it [Hansen et al, 2011].

The main objective of the Leonardo mission is to make the first ever significant direct radiative measurement of the Earth's Energy Imbalance with an accuracy of 0.1 W/m².

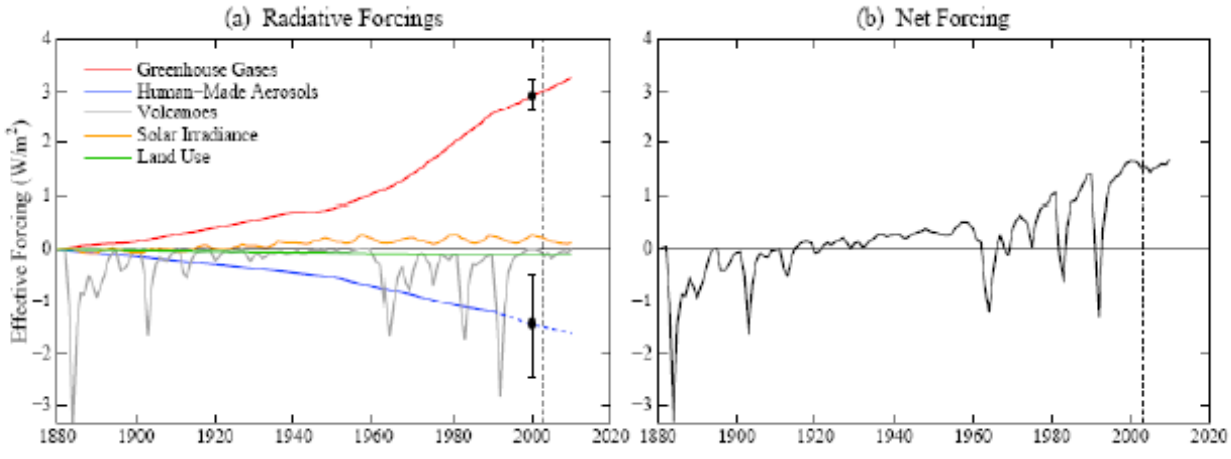

Figure 3: reproduction of figure 1 of [Hansen et al 2012]: left: radiative forcing components and right: net forcing.

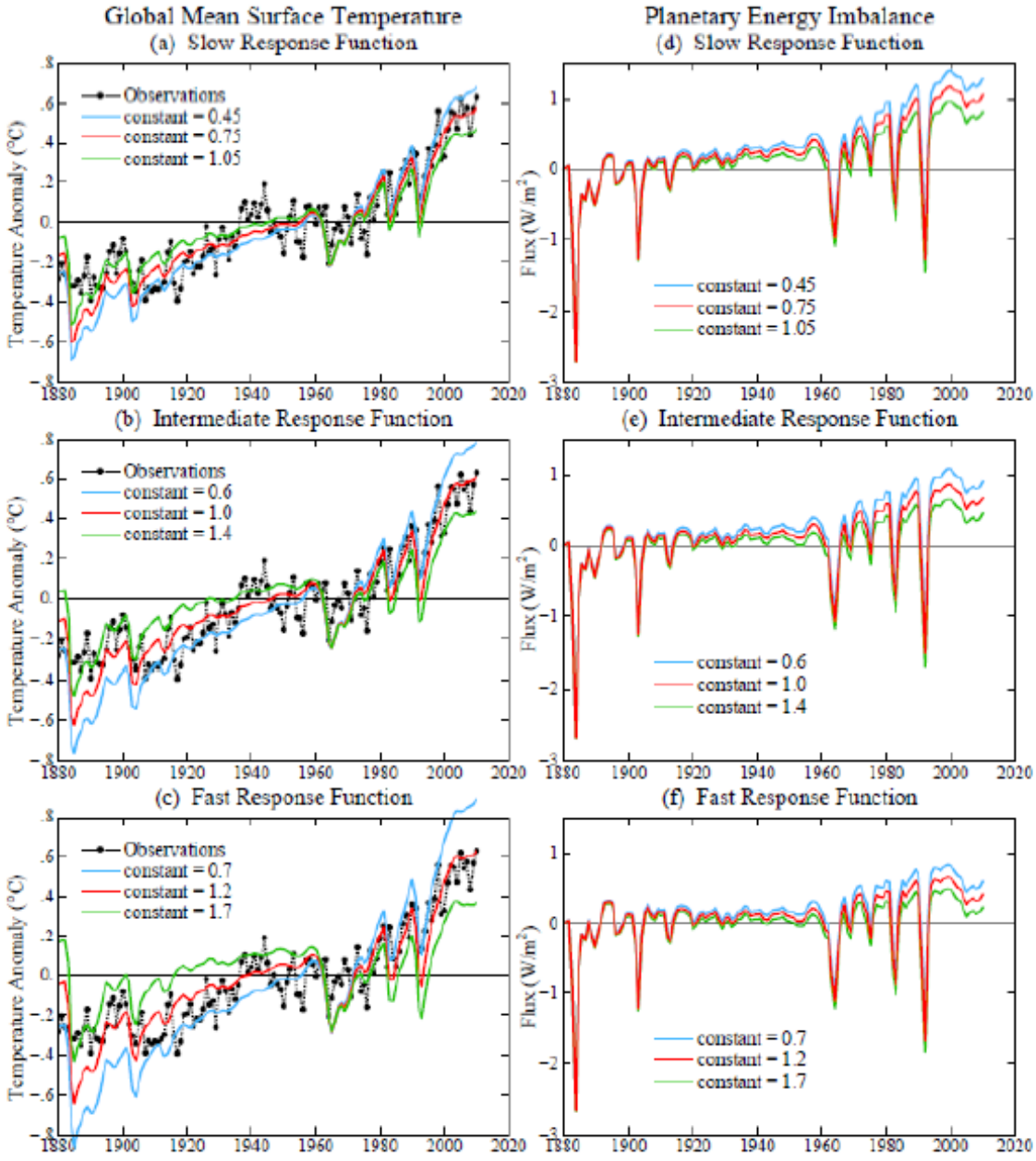

Figure 4: reproduction of figure 7 of [Hansen et al 2012]: the joint observation of global temperature change (left) and the Earth Energy Imbalance (EEI) (right) allow to determine the speed of the climate response function – which depends on ocean mixing – and the aerosol forcing. 'constant' is a multiplicative factor for the aerosol forcing of figure 3.

Currently two approaches exist for the measurement of the EEI [Trenberth et al, 2016]: 1) the direct approach through radiative measurements, 2) the indirect approach through the measurement of Ocean Heat Content (OHC). Both approaches currently have strengths and weaknesses.

The direct radiative measurement provides a good monitoring of the variability of the EEI with a stability better than 0.3 W/m²decade [Loeb et al, 2009] [Allan et al, 2017]. However, the absolute accuracy is quite poor with an estimated absolute value of the EEI of 4.3 +/- 4.9 W/m² [Dewitte & Clerbaux, 2017].

The indirect measurement of the EEI through the OHC provides a better absolute measurement of the EEI of 0.9 +/- 0.3 W/m² [Trenberth et al, 2016]. However, the noise level of the OHC is quite high, the long term stability is hindered by data sampling limitations [Lyman & Johnson, 2014], and there can exist errors due to the lack of sampling of ice covered oceans [Trenberth et al, 2016].

The fundamental reason why the absolute accuracy of the current direct radiative measurement of the EEI is poor, is that the EEI is the small difference of two large nearly equal terms of opposite sign: the incoming solar radiation and the outgoing total earth leaving radiation. Up to now the two large terms are measured with separate instruments, resulting in an addition of their calibration errors, which is larger than the small difference to be measured. We propose a breakthrough novel approach making measurements of the incoming solar radiation and the earth leaving radiation with exactly the same instrument, resulting in a true differential measurement of the EEI.

The second objective of the Leonardo mission is to make observations of the Total Solar Irradiance with an accuracy of 1 W/m².

For making the highly accurate differential sun-earth measurement, we need an absolute instrument which is capable of measuring both the solar irradiance and the earth irradiance accurately. The instrument of choice is a Wide Field Of View (WFOV) Electrical Substitution (ES) Cavity Radiometer (CR). The detector of a CR is a blackened cavity which absorbs nearly all incoming radiation. Following the ES principle, the absorbed optical power is measured by comparing it with an electrical power which has the same thermal effect.

The Leonardo CR will be pointed to the earth nearly continuously in order to provide a good sampling of the spatial and temporal variability of the earth leaving radiation. It will be pointed to the sun from time to time in order to use the sun as a calibration source for the earth measurements. The variation of the sun in between two solar calibration measurements will be well known from the operational TSI radiometers [Dewitte & Nevens, 2016] [Dewitte & Clerbaux, 2017], see figure 5. The solar spectrum is known from [Meftah et al, 2017].

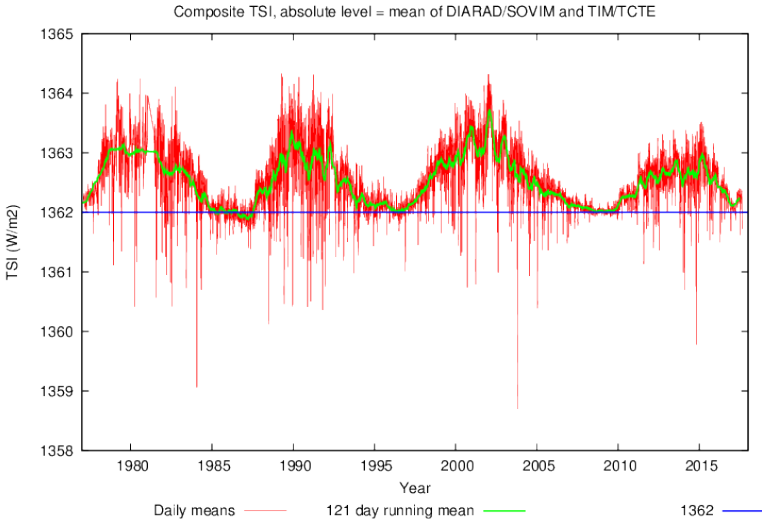

Figure 5: The Total Solar Irradiance and its variations following [Dewitte & Clerbaux, 2017].

When observing the earth from a low earth orbit satellite, the higher the required spatial resolution is, the lower the captured signal is. This is a disadvantage with respect to intercalibration with the sun. To put ourselves in the most favourable condition for sun-earth intercalibration, the Leonardo CR will measure the earth at the lowest possible resolution, this means it will measure from limb to limb as one measurement point. In that case it will also measure the true flux at satellite altitude, eliminating the need to model the angular dependency of the earth leaving radiation.

When pointed to the sun, the CR will measure a TSI of the order of 1362 W/m². When pointed towards the earth it will measure an earth leaving flux of minimum 200 W/m² for emitted thermal radiation during night up to maximum 500 W/m² for the total flux during daytime Thus the ratio between the sun and the earth measurements will be less than one order of magnitude. This is much more favourable than the intercalibration conditions proposed for Clarreo [Wielicki et al, 2013] or Truths [Fox et al, 2011].

The third objective of the Leonardo mission is to measure the outgoing ERB components of Reflected Solar Radiation (RSR) and Outgoing Longwave Radiation (OLR) with adequate statistical sampling of the monthly mean diurnal cycle, with global spatial sampling at a spatial resolution allowing the separation of cloudy and clear sky scenes.

Clouds are the most important modulators of the earth leaving radiation: when they occur, they locally increase the reflection of solar radiation and they decrease the emission of thermal radiation. Figure 6 illustrates the ERB fields influenced by the presence of clouds as measured by Ceres following [Dewitte & Clerbaux, 2017]. The size of the CR footprint will be of the order of 5900 km diameter. This is too large to discriminate the effect of individual clouds and to separate cloudy from clear sky scenes. Also it is useful to separate the total earth leaving radiation according to wavelength. Reflected solar radiation also known as ShortWave (SW) radiation, has wavelengths below 4 micron, and maximum intensity around 500 nm. Emitted thermal radiation also known as LongWave (LW) radiation, has wavelengths above 4 micron and a maximum intensity around 11 micron.

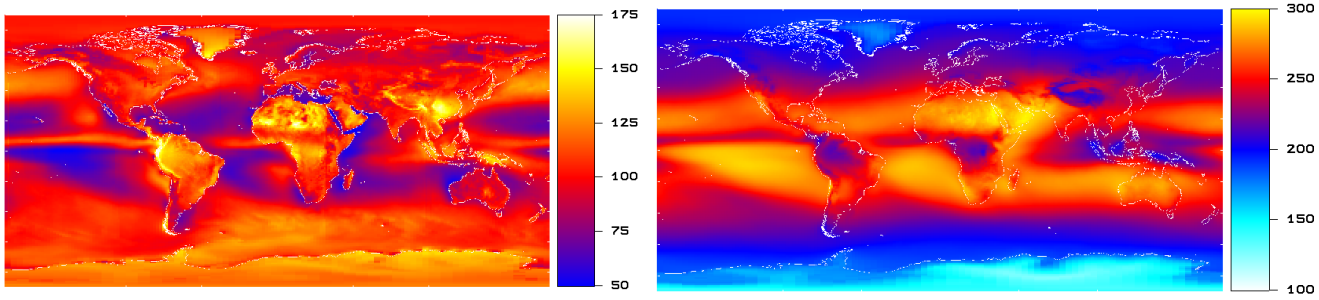

Figure 6: Reflected solar flux (left) and emitted thermal flux (right) as measured by Ceres for the period 2000-2010 following [Dewitte & Clerbaux, 2017]. The scale is in W/m².

For cloud/clear sky and SW/LW spectral separation, besides the CR, Leonardo will have wide field of view SW and LW cameras. At a given moment in time the CR and the cameras will observe the same part of the earth. Within the cavity footprint, these cameras will characterise the angular distribution of the SW and LW radiation. Based on radiative transfer calculations, it will be possible to estimate the Reflected Solar Radiation (RSR) and Outgoing Longwave Radiation (OLR) at the camera pixel level with relative low accuracy around 5%. Integrated over the CR, the camera based OLR and RSR can be recalibrated to the CR accuracy of 0.1/340 ≈ 0.03% or 300 ppm. First, the OLR will be recalibrated using night time measurements. Next, the RSR will be recalibrated using daytime measurements.

The different angular distribution of the solar radiation entering the CR during solar calibration, and the earth radiation entering the CR during earth observation will be the major source of uncertainty of the sun-earth intercalibration by the CR. As the SW and LW cameras will characterise the angular distribution of the earth radiation entering the CR, they will contribute to increasing the accuracy of the CR.

The accuracy of the broadband estimate from the WFOV cameras can be improved by using spectral information provided by the third Leonardo instrument, which will be a cross-track scanning broadband spectrometer. This spectrometer will also allow the detection of clouds and the measurement of their optical properties like cloud optical depth, cloud top temperature and cloud phase.

One of the applications of the measurement of the spatial distribution of the outgoing ERB terms is the characterisation of the hemispheric imbalance of the ERB [Loeb et al, 2015]. The interhemispheric asymmetry is a fundamental characteristic of climate [Frierson et al, 2013] and it is linked to pervasive and systematic model biases [Haywood et al. 2016] [Stephens et al, 2015].

The fourth objective of the Leonardo mission is to make joint measurements of the Aerosol Optical Depth (AOD), allowing to make an assessment of the direct aerosol radiative effect.

Aerosols, through their direct radiative effect and through their diverse and complex indirect effects, are a major source of uncertainty in the interpretation of the ERB and climate change [Boucher et al, 2013] [Rosenfeld et al, 2014]. Important long-term changes in atmospheric aerosol load are revealed in the so-called global dimming and brightening [Wild, 2009]. One of the most important consequences on climate may be the indirect aerosol effect on the general circulation. Since anthropogenic aerosol predominantly affect the northern hemisphere, it can be expected they cool the Northern Hemisphere, which through the above mentioned interhemispheric asymmetry seems to cause a southward shift of the ITCZ implying significant climate change in the tropics and the extratropics [Rotstayn & Lohmann, 2002] [Brocoli et al 2006] [Chang et al 2011] [Bollasino et al, 2011] [Booth et al, 2012] [Hwang et al 2013] [Chung & Soden, 2017] [Dewitte & Clerbaux, 2017].

In the Leonardo mission the presence of aerosols in clear sky conditions will be measured through the Aerosol Optical Depth (AOD), which can then be correlated with ERB variations in order disentangle and understand the aerosol direct and indirect effects on the ERB.

AOD retrieval algorithms are reviewed in [Mischenko, 2010]. The Leonardo AOD retrieval will make use of the multiangle observations of the SW WFOV camera and of the spectral information of the spectrometer, particularly measurements at short (blue) wavelengths.

The fourth objective of the Leonardo mission is to make joint measurement of the atmospheric and surface parmeters that influence the ERB.

The spectrometer will provide information about clouds, surface spectral albedo and emissivity, surface and atmospheric temperature, and the greenhouse effects of water vapour, CO_2 and ozone.

2.2 Mission duration and relation to other planned or existing missions

The minimum Leonardo mission duration will be 6 years. This corresponds to the minimum averaging period to allow a meaningful comparison with Ocean Heat Content measurements [Trenberth et al, 2016]. It will also allow the characterisation of the interannual El Nino / La Nina variability.

Leonardo will fly in synergy with existing wide swath instruments in Sun Synchronous Orbits (SSO's). In the afternoon orbit these SSO synergy instruments are the Ceres instruments on NPP or NOAA-20, or the Ceres

follow-on RBI on JPSS-2. In the morning orbits these SSO synergy instruments are the AVHRR instruments on Metop or the follow-on instrument Metimage on Metop SG. As Leonardo will fly in an orbit with slow precession it will come in and out of phase with the SSO instruments, allowing the intercalibration of the SSO instruments during the time periods when they are in phase with Leonardo.

Figure 7 illustrates the latitude/local time sampling of an idealised "triphase" SSO constellation and a precessing Leonardo orbit. The triphase constellation consists of a morning orbit – with 10:00 LTAN (Local Time of Ascending Node), covered by the European meteorological satellites, an afternoon orbit – with 14:00 LDTN (Local Time of Descending Node), covered by the US meteorological satellites, and the early morning orbit – with 6:00 LTDN, which will in the future be covered by Chinese meteorological satellites, starting with FY3E with foreseen launch in 2019 [Hong et al, 2016].

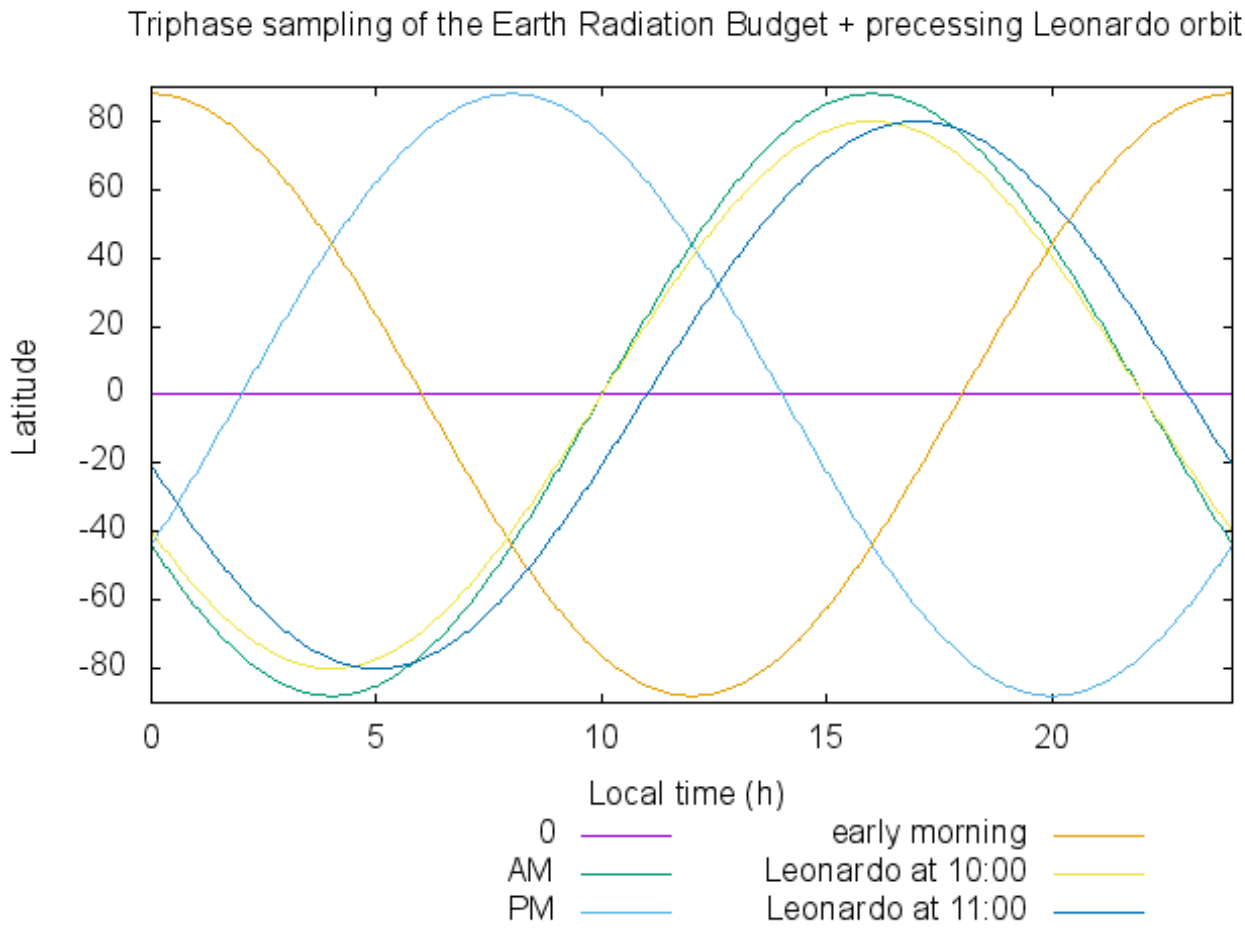

Figure 7: Sampling of local time versus latitude for an idealsed triphase SSO constellation complemented with a precessing Leonardo orbit.

Through its orbit precession Leonardo will provide a statistical sampling of the diurnal cycle of the ERB at the seasonal time scale. In synergy with the calibrated SSO instruments, Leonardo will provide a statistical sampling of the diurnal cycle at the monthly time scale.

2.3 Observation requirements

Leonardo will observe the following geophysical variables:

during solar calibration periods of 5 orbits every 83 days:

1) the instantaneous Total Solar Irradiance with an accuracy of 1 W/m² and a temporal sampling of 2 minutes

during earth pointing which should cover at least 95 % of the mission time:

2) the instantaneous Total earth leaving radiative flux measured at satellite altitude with an intercalibration accuracy relative to the Total Solar Irradiance of 0.1 W/m² and a temporal sampling of 2 minutes
3) Reflected Solar and Emitted Thermal radiance at 3.9 km resolution at nadir compatible with the Total earth leaving fluxes at satellite altitude
4) cloud mask, cloud optical depth, cloud top temperature and cloud phase at 4.4 km resolution at nadir
5) Reflected Solar and Emitted Thermal flux at 10 km resolution at nadir compatible with the Total earth leaving fluxes at satellite altitude
6) under clear sky conditions: Aerosol Optical Depth at 4.4 km resolution at nadir
7) under clear sky conditions: surface spectral reflectance and emissivity, surface and atmospheric temperature, column integrated amounts of WV and ozone at 4.4 km resolution at nadir

for the mission as a whole:

8) 6 year mean of the Earth Energy Imbalance with an accuracy of 0.1 W/m²

2.4 Scientific Readiness Level status

In this proposal a first iteration of the top-level Leonardo scientific and observation reuirements are formulated. These requirements serve to reach the user goal of measuring the Earth Energy Imbalance and the factors that are changing it [Hansen et al, 2011]. Based on the observation requirements a justified selection of the technical Leonardo mission elements (instruments, orbit, …) is made. Thus the Leonardo mission idea is currently at SRL-3 according to [ESA,2015].

2.5 Roadmap to achieve SRL 5 at the end of Phase A

In order to reach SRL 5 – an end to end simulator – the generic steps outlined in figure 8 are needed.

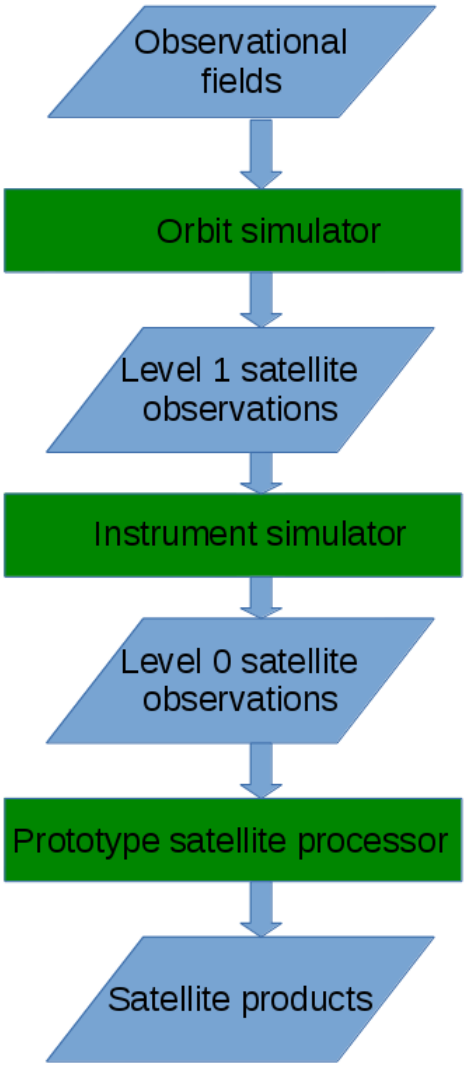

Fig 8: Generic flowchart for end to end simulator of satellite mission.

Specifically for the Leonardo mission the elements in this flowchart need to be developed as described below. No particular blocking elements prohibit these developments until the end of Phase A. Experience in the proposing team with similar pre-flight satellite mission simulations is available from the Gerb [Harries et al, 2005] and Earthcare [Illingworth et al, 2015] projects.

Observational fields

The Ceres project [Wielicki et al, 1996][Loeb et al, 2009] provides the best estimate of the observational fields of the ERB broadband fluxes at 20 km resolution. From 2003 to the present (early 2018) Ceres is available on the morning satellite Terra and the afternoon satellite Aqua. The multispectral imager MODIS provides auxiliary information such as cloud properties [Minnis et al, 2011] [Platnick et al, 2015] and aerosol characterisation [Sayer et al, 2014]. The Ceres SYN and EBAF products [Rutan et al, 2015] use additional data from geostationary imagers, providing a realistic diurnal cycle.

Orbit simulator

For the Leonardo mission a simulation of the precessing Leonardo orbit and the particular viewing geometry of the CR, WFOV cameras and cross-track scanning spectrometer need to be developed.

Instrument simulator

For the Leonardo mission in particular the detailed functioning of the CR needs to be simulated in order to demonstrate its accuracy. It is also advisable to build an early hardware prototype of the CR and compare its laboratory performance with the simulations. The simulations of the CR include the flow of thermal energy in the cavity sidewall and the functioning of the local Electrical Substitution servo algorithm.

Prototype satellite processor

The Leonardo prototype processor needs to be developed based on the experience with existing instuments described below.

The most innovative Leonardo instrument is the Cavity Radiometer, which aims to provide a breakthrough accuracy for the Earth Energy Imbalance measurement. The design of this instrument builds further on existing Cavity Radiometers for the measurement of Total Solar Irradiance and the Earth Radiation Budget from space. These have a long history, which is reviewed in [Dewitte & Clerbaux, 2017]. In particular, the PI institute, RMIB, has made 11 different space flights with 6 different Cavity Radiometers for the measurement of Total Solar Irradiance [Dewitte et al, 2004] [Mekaoui et al, 2010] [Dewitte et al, 2012] [Meftah et al, 2014] [Dewitte & Nevens, 2016]. The adaptation of this type of radiometer to the Leonardo CR requires some technical improvements, which are detailed in the technical chapter. Experience with the monitoring of the variability of the ERB with CR's exist from ERBE [Wong et al, 2006] [Allan et al, 2017].

The high resolution ERB measurement techniques and data processing methods have strong heritage from the Ceres [Wielicki et al, 1996] [Loeb et al, 2009], Gerb [Harries et al, 2005] [Dewitte et al 2008] and Earthcare BBR [Illingworth et al, 2015] [Caldwell et al, 2017a] [Caldwell et al, 2017b] projects. The PI and several CoIs have experience with these projects.

The cloud retrievals needed for Leonardo have heritage from the Ceres [Minnis et al, 2011], Modis [Platnick et al, 2015] and CMSAF [Karlsson et al, 2012] projects.

The AOD retrieval needed for Leonardo has heritage from the techniques reviewed in [Mischenko, 2010].

The retrieval of surface and atmospheric parameters needed for Leonardo has heritage from SEVIRI and IASI [Liuzzi et al, 2016] [Masiello et al 2015].

3. Technical Concept

3.1 Orbit

The nominal Leonardo orbit will have an altitude of 750 km and an inclination of 80° . This results in a slow precession of the satellite orbit relative to the sun of 2.2°/day. The full diurnal cycle will be sampled in 83 days.

The limb to limb viewing angle is 126°. The limb to limb viewing footprint is 5900 km.

3.2 Cavity Radiometer

As a baseline the Cavity Radiometer (CR) will be designed, a prototype will be built, and the metrological characterisation will be done by RMIB in partnership with LATMOS and VUB. The Flight Model will be constructed by LATMOS or by QS. A collaboration RMIB-LATMOS was followed for the construction of the SOVA-Picard instrument [Meftah et al, 2014]. A collaboration RMIB-QS was followed for the construction of the DIARAD/VIRGO TSI radiometer [Dewitte et al, 2004].

The nominal design of the CR is illustrated in figure 10. A precision aperture of 1 cm diameter allows solar or earth radiation to enter into the cavity. A baffle limits the unvignetted field of view to 130°. The cavity shape is aprroximately spherical similar to [Kim et al, 2014], such that the distance of the cavity side wall to the precision aperture is approximately constant and equal to 5 cm. The cavity side wall is covered with Vacuum Aligned Carbon NanoTubes (VACNT) with VIS and IR reflectance smaller or equal to 0.4 %. The resulting cavity reflectance is smaller or equal than 40 ppm. On the outer side of the cavity multiple electrical heater and temperature sensors are connected. The power in the heaters will be regulated by a digital servo system such that the measured temperatures remain constant. A variation of an unknown incident optical power absorbed at a given point in the cavity will then be measured by the opposite variation of electrical power needed to keep the local temperature constant. The electrical power is measured by a separate measurement of voltage and current. The cavity is put in a housing which is thermally regulated such that the only variable entrance to the cavity arrives through the precision aperture. By the use of a Gallium phase change cell, the housing can be kept at a constant absolute temperature of 29.765 °C. The measurement electronics is placed inside the thermal housing for an optimal accuracy of the electrical power measurements.

The expected dominating error source for the sun-earth intercalibration is the spatial non-uniformity of the cavity. This non-unformity can be characrterized on-gound with a laser beam or in-flight using the sun as a point source. The spatial non-uniformity is determined by the “thermal voltage divider” formed by the internal thermal resistance Rth,int of the cavity side wall and the external thermal resistance Rth,ext between the cavity and the housing. Rth,int will be of the order of 0.1 K/W, and Rth,ext will be of the order of 40 K/W, resulting in a non-uniformity of 0.25% or 2500 ppm. The WFOV cameras will be used to caracterise the spatial distribution of the incoming radiation with an accuracy of 5%. The resulting spatial non-unformity error of the CR will be of the order of 125 ppm. The total sun-earth intercalibration error of the CR will be of the order of 150 ppm. This is a factor of 2 lower than the required 300 ppm.

Other critical elements are the use of VACNT black, and of the Ga phase change cell for maintaining a constant absolute temperature. Both of these technologies have already been demonstrated in-flight from the RAVAN

cubesat [Swartz et al, 2015]. VACNT is available from Surrey NanoSystems (SNS) as 'Vantablack', see figure 11 (right) for the IR reflectance.

A prototype of the CR should be built early on including the VACNT black and the Ga phase change cell. The distributed ES should be demonstrated, the spatial non-uniformity should be characterised and the achievable accuracy should be validated.

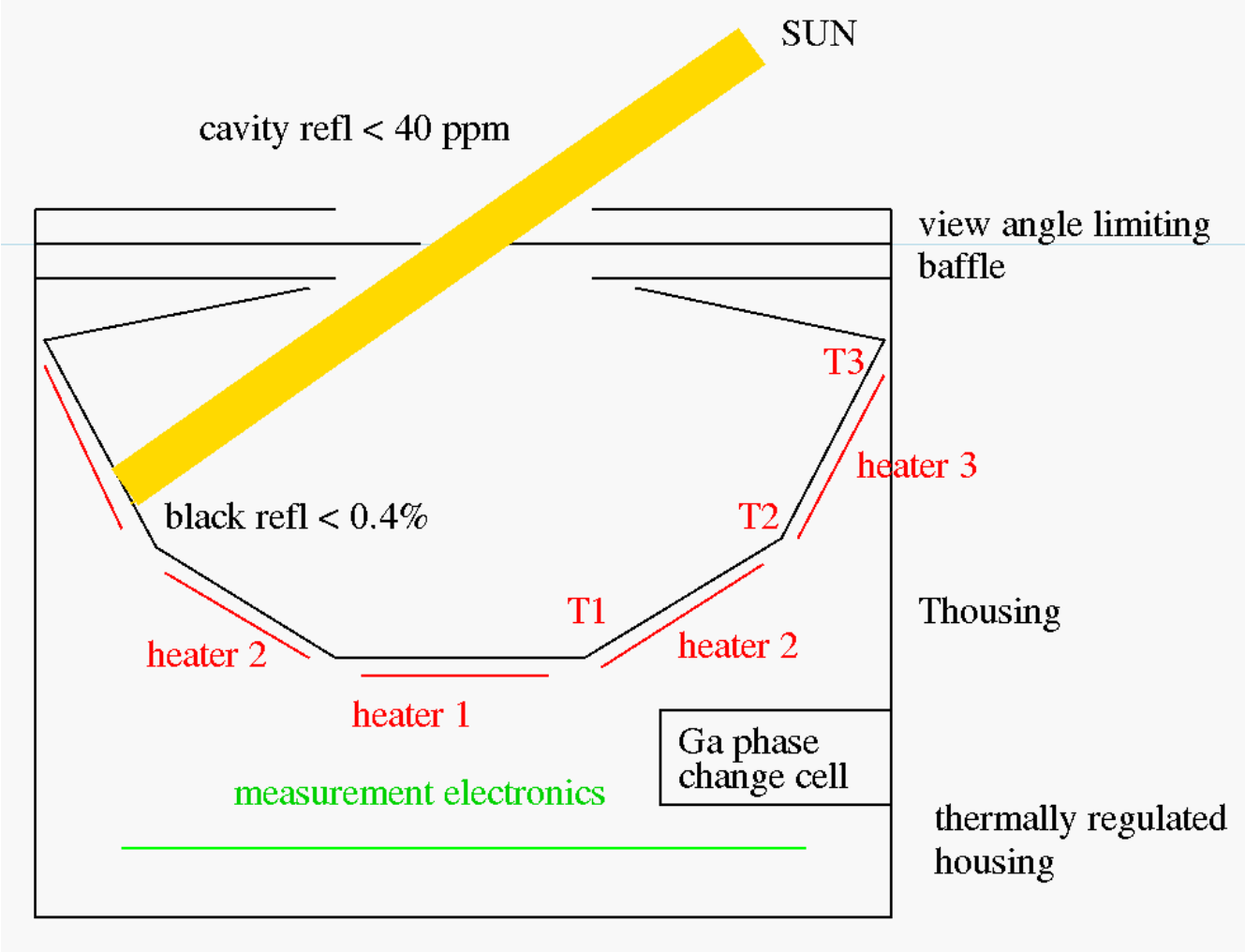

Figure 10: Cavity Radiometer design.

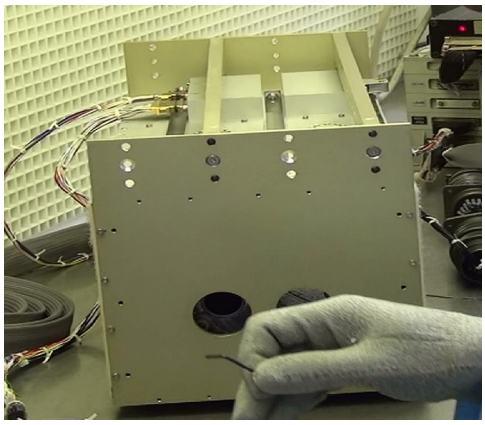

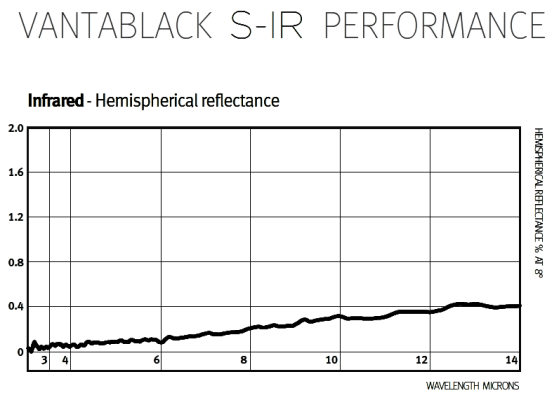

Figure 11: Left: RMIB Sova1 radiometer that has flown on Eureca.. Right: IR spectral reflectance of Vantablack S-IR from SNS.

3.3 Wide Field Of View Cameras

The Wide Field Of View cameras can be provided either by Jena Optronik (JOP) or by RAL Space.

The SW camera will consist of a fish eye lens placed in front of a backlit CCD detector with spectral response in the range of 400 to 900 nm. It will be possible to place a shutter in front of the camera to protect it against direct solar illumination during solar calibration pointing. The SW camera is not critical as it has a strong heritage from existing star trackers.

A star tracker produced by JOP, a backlit CCD produced by E2V together with typical spectral responses are shown below.

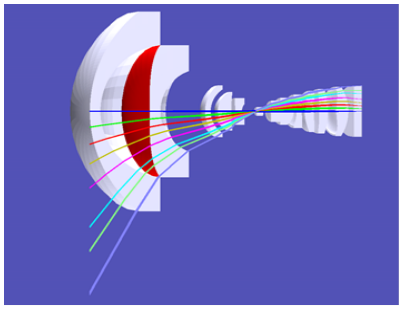

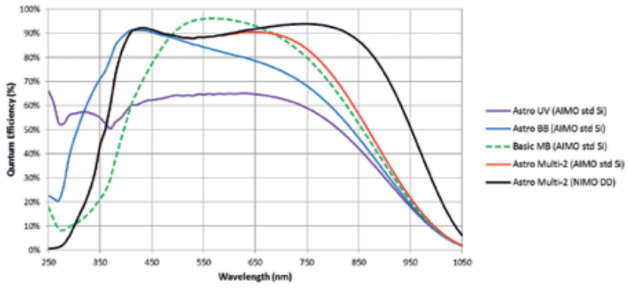

Fig. 12: JOP star tracker (left), wide field of view lens optical design (middle) and typical spectral responses of an E2V back illuminated CCD (right).

For maximum sensitivity to aerosols, a UV enhanced spectral response will be favoured.

For a 1024X1024 pixel CCD at an altitude of 750 km covering a 141° field of view the nadir resolution of the WFOV camera will be 2.9 km. One image will be captured every 0.2 s, with a Signal to Noise Ratio (SNR) around 170 for a Top Of Atmosphere (TOA) reflectance of 0.3 and overhead sun. As a baseline, the images will be transmitted to the ground at a rate of maximum 50 Mbit/s. For comparison with the CR, the images will be convolved on the ground with the CR time response and integrated over 60 s, resulting in a SNR around 3000.

The LW camera will consist of a fish eye lens placed in front of an uncooled microbolometer detector array with spectral response in the range of 8 to 14 micron. It will be possible to place a blackened shutter with temperature sensor in front of the camera as a blackbody calibrator or to protect it against direct solar illumination during solar calibration pointing.

A Megapixel uncooled array produced for ESA by Xenics and INO is shown below.

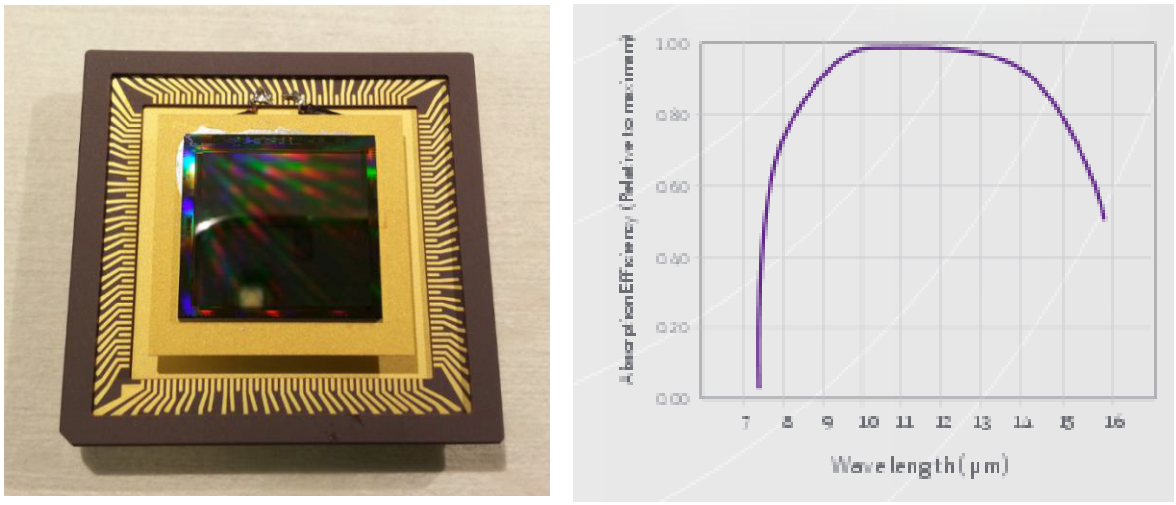

Figure 13: Megapixel uncooled microbolometer array (left) and typical spectral response (right).

The design of a LW fish eye lens is not standard, but it does not pose principal problems. A ground LW fish eye lense has been produced by [NEOS].

During Phase A an optical design of the lenses should be made, and prototype cameras using breadboard electronics have to be realised.

3.4 Scanning spectrometer

As a baseline the scanning spectrometer will be provided by RAL Space.

Figure 14 (left) shows the layout of the scanning spectrometer. The rotating scan mirror at 45-degree angle-of-incidence provides a continuous scan in the across-track direction, from limb-to-limb, with scan range between +/-60 degrees from nadir. At further scan positions beyond the limb it also provides the needed calibration views; an integrating sphere (IS) which uses in-built lamps for its SW illumination, a BlackBody (BB) as LW calibration source, and possibly also space-view. The earth scanning is illustrated in figure 14 (right).

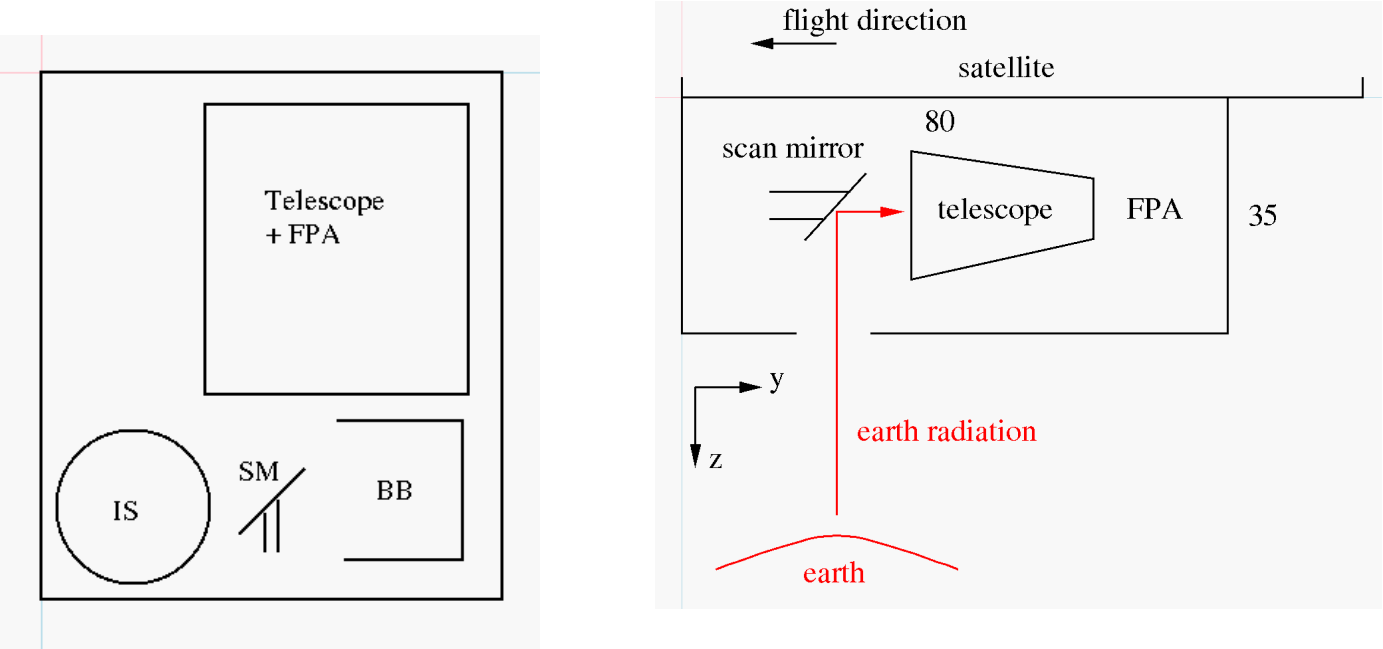

Figure 14. Left: layout of the spectrometer. SM=Scan Mirror, IS= Integrating Sphere, BB=Blackbody, FPA = Focal Plane Array.. Right: Earth scanning by the spectrometer. The indicated dimensions are in cm.

The spectrometer uses two-dimensional array detectors, to obtain instantaneous spatial-sampling in the along-track direction, plus spectral-sampling in the other lateral direction. For non-nadir scan positions the spectral-direction becomes increasing rotated with respect to along-track due to the scan geometry.. The required spectral-range is 300 nm to 4 micron in SW and 4 to 20 micron in LW, and suitable spectral-resolution would be ~10 points across each band. The suitable detector for LW is a micro-bolometer array such as is used for the LW-Camera, but with the addition of a broad-band black coating (such as used on GERB and BBR) to give the spectral range. For the SW band too, the required broad band range means that a blackened micro-bolometer array is the preferred solution. Depending on the design, and available array sizes, a single array detector may be able to cover both bands. This would have some advantages for cost and simplicity, whereas the advantages of using separate arrays are that the optics and detectors can be optimised separately for SW and LW as described below.

The use of bolometer arrays limits the pixel response speed, and this drives the possible choices of scan rate and ground-sampling distance (GSD). For a typical 10ms required dwell time per spatial element, a suitable GSD is ~4.4km. For a full-rotation scan (i.e. 360 degrees) at this speed, the scan period is ~10s, corresponding to an along-track repeat distance of ~80km. Thus a suitable binning size for the detector array in this direction is 80km/4.4km ~18 elements. It is also possible to use and alternating scan (e.g. oscillating mechanism), in which case the 2-D detector array would over-sample the earth. Also a variable-speed scan may be considered, to scan more slowly when viewing the calibration sources, to optimise the source geometry. For the choice of detector array format, to achieve the need of ~18 x 20 bins (spatial x spectral), suitable detectors could be e.g. 128^2 pixels or larger, with suitable binning. This binning will be done on-ground in order to achieve required spatial co-registration between spectral channels, as for the Earthcare BBR.

For the optical design, with the above image format the instantaneous-FOV is ~ 6 degrees along-track, and with both bands needing a broad spectral-range this probably requires an all-mirror design. There are two possible spectrometer types for a compact system:

1) Imaging camera with square FOV, plus linear-variable-filter (LVF) at the detector focal plane

2) Imaging grating-spectrometer (with entrance-slit oriented in along-track direction), as used for example in MERTIS

There are pros and cons for each of these options. For the LVF scheme the imaging format would then be as shown in figure 15, with the spectral direction being parallel to the scan-direction at nadir, and FOV's of the two bands sitting side-by-side. For the use of LVF the system is simpler, but the requirement for a two-dimensional FOV of 6x 6 degrees is difficult for aberration control in a mirror system as compared to one-dimensional FOV. Also the implementation of the LVF's close to the detector surfaces is a technical challenge for the detector procurement as it is a customisation (packaging issue). For the LW band the LVF may be difficult to design as fewer multi-layer and substrate material choices are available for longer wavelengths.

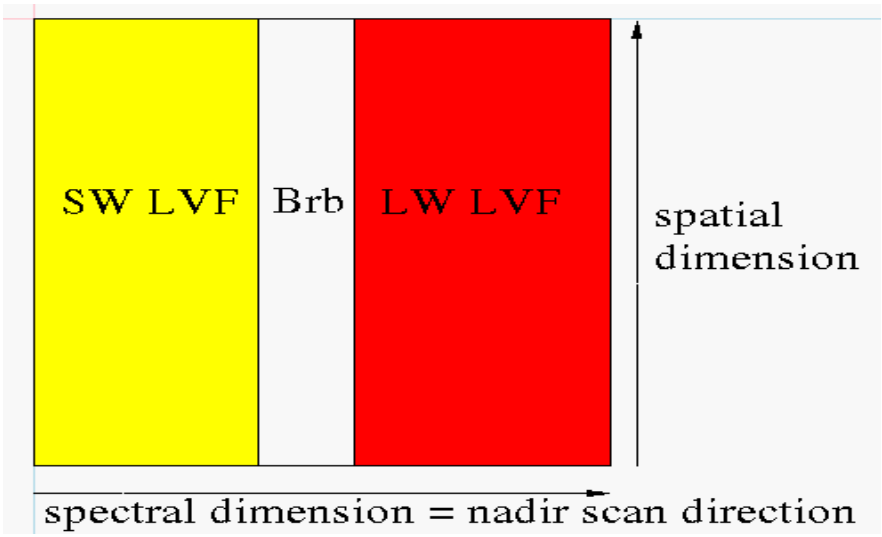

Figure 15: Spectrometer FPA which consists of Brb detector array with separate SW and LW LVF.'s.

For the grating-spectrometer solution, the MERTIS heritage [Hiesinger et al, 2010] is close to an existing solution; a three-mirror-anastigmat can provide the linear-FOV imaging the earth to an entrance-slit, and an Offner-relay with grating forming one of the mirrors, can produce the needed spectral-range on a 2-D bolometer array (120 x 160 in MERTIS). This would also be a compact design, for ~2cm aperture, and with fast optics in order to limit the diffraction effect in the LW (F/2 in MERTIS and 35um pixel size). For either type of spectrometer there are trade-offs for use of a single array or separate arrays for SW and LW within a single spectrometer, or to have fully separate side-by-side spectrometers for each band, in order to optimise each separately. For the LVF option, the use of separate arrays would ease the LVF design and detector packaging tasks. For both types of design the use of separate arrays would also allow detector performance to be optimised separately, but the use of a single array has other advantages. For example if a broad-band black that covers both bands is used (as in BBR), this would aid cross-calibration between SW and LW.

As a baseline the LVF option with a single detector array will be choosen. In the spectral dimension the detector array will have 18 pixels, of which 7 will be used for SW channels, 3 for non filtered Broadband (Brb) channels, and 8 for LW channels. The nominal spectral channels and their information content is given in the table below.

SW channel	Range (nm)	Information	LW channel	Range (micron)	Information
SW1	300-500	Ozone, aerosols	LW1	6-7	UTH
SW2	500-700	VIS Surface albedo, cloud optical depth	LW2	7-8	MTH
SW3	700-900	NIR surface albedo, WV	LW3	8-9	Cloud top particle size, cloud phase
SW4	900-1100	NIR surface albedo, WV	LW4	9-10	Ozone
SW5	1100-1300	NIR surface albedo, WV	LW5	10-11	Surface & cloud top temperature
SW6	1300-1500	WV	LW6	11-12	Column WV, thin cirrus and dust/ash clouds
SW7	1500-1700	Cloud particle size	LW7	12-13	Lower trop. temperature
			LW8	13-14	Mid trop. temperature

The telescope needs to have a relatively wide field of view of 6° by 6°. This can be achieved by an axisymmetric Korsch telescope [Korsch, 1977] or by a non axisymmetric one using freeform design and manufacturing techniques [Chrisp et al, 2016]. Figure 16 illustrates the [Chrisp et al, 2016] optical design of a 10° x 9° telescope with 18x18 cm² entrance pupil, 35.7 cm focal length, f-number 2 and 14 micron RMS spot size. The capacity to design such a telescope is available both at RAL and at VUB, and the capacity to manufacture it is available at VUB.

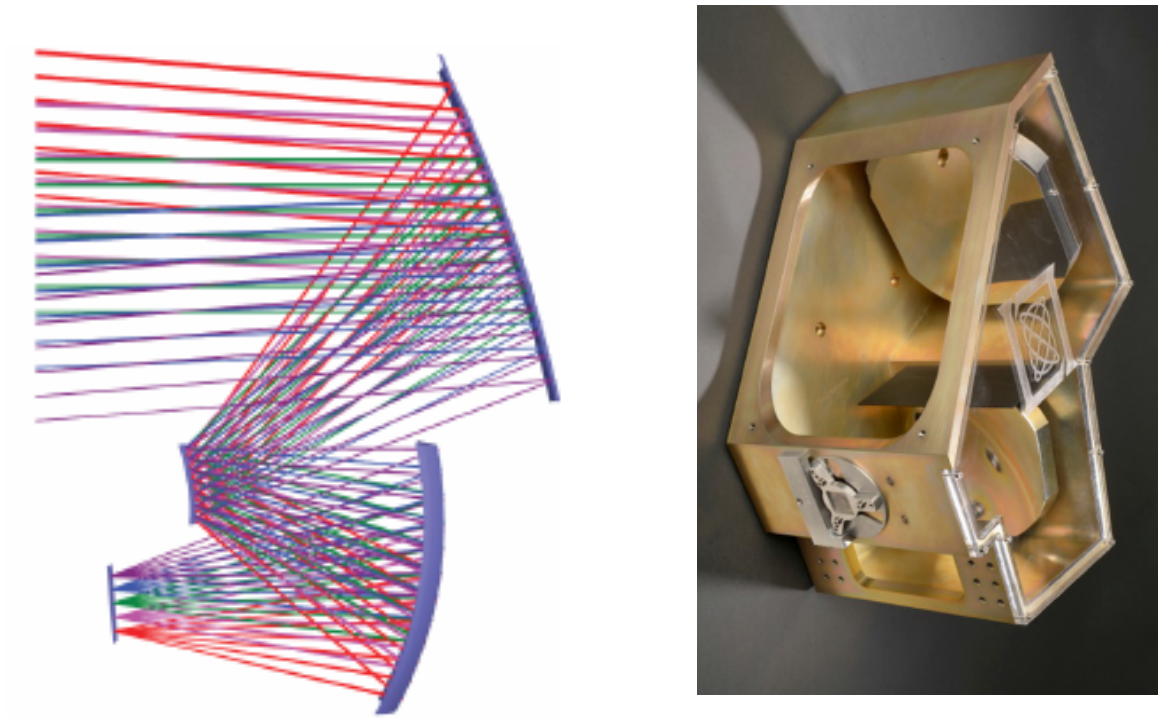

Figure 16. Freefrom 10° x 9° telescope following [Chrisp et al, 2016]. Left: optical design. Right: demonstration telescope.

The spectrometer design has heritage from the AVHRR, Gerb and Earthcare BBR instruments.

The developments that are needed to reach TRL-5 by end of Phase B1 are described below.

Detectors sub-system
The design uses existing micro-bolometer arrays previously developed (MERTIS, BBR). However there are new and custom features in the detector, in the required black coating, and in the read-out electronics needed for bolometer radiometric signal sampling, for the non-chopped scheme and 2-D format used (design of detector read-out integrated circuit and front-end electronics).
The hardware models needed to reach TRL are: 1) a Blacking qualification detector. This would use the vendor's normal detector packaging and read-out scheme, but would include the chosen black coatings. The coating aspects of deposition process, and pixelation (e.g. laser trimming post-blacking) have to be addressed. This detector would be tested for effects of the black on responsivity, speed, and spectral response. Also full environmental testing

2) a Development model detector. This would be representative of the detector format, read-out scheme (ROIC) and front-end-electronics (up to digitisation of the per-pixel radiance-response waveform). Also within a focal-plane package size required by optical design. This would be to demonstrate readout functionality and performance (e.g. dynamic-range, noise, cross-talk) at required read-out rate.

Optics sub-system
The LVF is likely to be a custom design for the geometry and band-pass values required, especially for the LW. The design, manufacture and characterisation of development models of each LVF is needed . This would include selection of suitable materials, including radiation-hardness and other environmental characteristics. The testing would include optical and spectral tests (requiring monochromator sources), as well as environmental tests.

The diffraction grating. This is a specialist custom component. For the LW it requires single-point-diamond turning of al-alloy on a spherical convex surface (MERTIS design). For SW the same technique may be used, or use of photo-lithography with holographic design. In both cases the design needs to be demonstrated and such custom optics have long lead times (~ 1year). Development models of each grating need to be made, and characterised to demonstrate their spectral-imaging performance (again using monochromator). For this the complete Offner system (3 mirrors) is needed plus suitable detector.
Breadboard model instrument
For which ever optical design is used, the DM's of the LVF or the grating, and the DM detector, should be brought together with a DM optical system to realise a full breadboard of the whole spectrometer, and this then characterised as a prototype instrument. This would use laboratory calibration sources; integrating-sphere for SW and black-body for LW. The characterisation would be for functionality (image read-out, data-rates), end-to-end performances (sensitivity/SNR, spatial and spectral resolution, cross-talk, stray-light background). This breadboard would not need to be designed for space environment tests.

Mechanism sub-system.
Although several mechanism and encoder types may exist for the required scanning, depending on the options it is likely that qualification model of the mechanism and drive electronics are needed. This is to demonstrate the custom aspects of this scanner, such as dynamic performance in closed-loop (e.g. linearity, jitter), and functionality such as variable-speed operation. A mechanism life-test model may be needed and is required early if this aspect has to be de-risked within phase-B1.
The on-board calibration sources are not considered as needing pre-developments to reach TRL-5.

3.5 Satellite

As a baseline a Proba satellite developed by Qinetiq Space (QS) will be used. Current Proba satellites in space are Proba 1, Proba 2 and Proba V. Figure 17 (left) shows the Proba V satellite during its integration on the laucnher. Planned Proba satellites under development are Proba 3 and Altius. As a baseline the Proba P400 platform will be used, this is an evolution of the Proba platfrom which is currently under development. The P400 has the following typical technical capabilities:

Mission design lifetime: 7 years

Payload mass capacity: 100 kg

Orbit average P/L power: depends on orbit and solar panel configuration. A preliminary analysis for the Leonardo configuration with 5 solar panels on the zenith side for power generation in the noon/midnight orbit and one additional side solar panel for power generation during the dusk/dawn orbit indicates 100 W EOL is achievable for all local equator crossing times.

External P/L volume: the Leonardo instruments can be accomodated, see CAD on figure 17 (right)

Data storage: up to 2 Tbit

Downlink: 400 Mbit/s

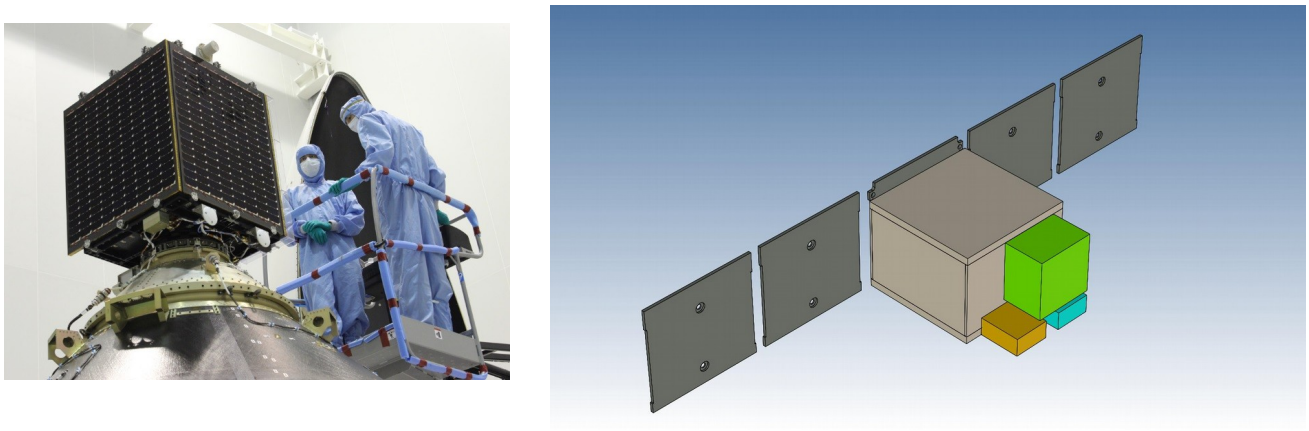

Figure 17: Left: Proba V satellite during integration on launcher. Right: Preliminary Leonardo CAD with payload instruments accommodated on the nadir side and solar panels on the zenith side for power generation during the noon/midnight orbit. An additional solar panel needs to be added on the side for power generation in the dusk/dawn orbit.

3.6 Pointing modes

The satellite will have three pointing modes:

1) In the default nadir pointing mode, the payload will be pointed towards the earth.

2) In solar calibration mode, the payload face will be pointed towards the sun, and all instruments except the Cavity Radiometer (CR) will be in a state where they are not harmed by direct solar exposure. At least during a part of the orbit, the earth should be completely out of the field of view of 130° of the payload face. For the characterisation of the CR spatial non uniformity the pointing angles relative to the sun should be configurable.

3) During deep space pointing the sun and the earth are out of the field of view of 130° of the payload face. Deep space pointing can be performed during the night part of the sun pointing orbit.

The Leonardo pointing modes are illustrated in figure 18.

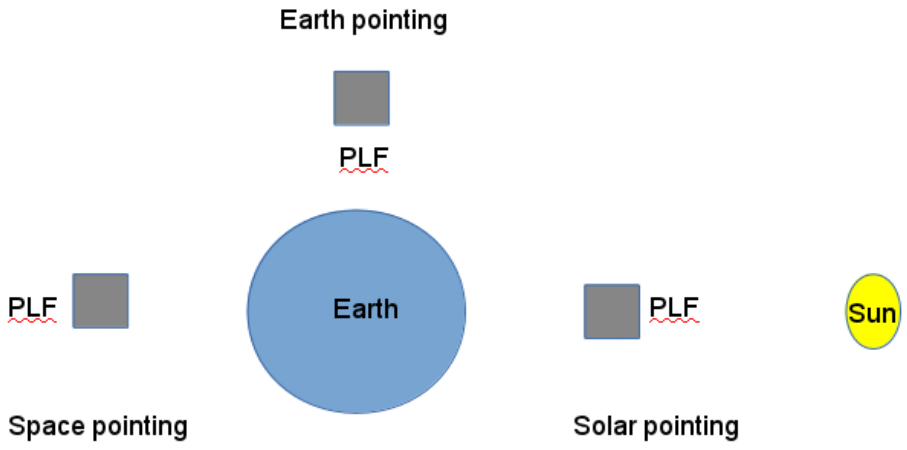

Figure 18: Leonardo pointing modes: earth pointing, solar pointing and space pointing. PLF = Payload Face.

The pointing should be accurate to 1° and the pointing knowledge should be accurate to 0.01°. The Proba satellite can deliver the required pointing modes and accuracies.

3.7 Thermal stability

The thermal stability will be controlled by passive design at satellite level, and where needed by active control at payload instrument level. A preliminary thermal analysis indicates that over a year the satellite mean temperature will vary between -7 °C and 20 °C. The worst case orbital temperature variation will be +/- 6° C.

3.8 Payload

The estimated resources needed for the payload are

	Power (W) including 20% instrument margin	**Mass (kg) including 20% instrument margin**	**Datarate (Mbit/s) including 20% instrument margin**
Spectrometer	24	28.8	2.4
WFOV cameras	23	23	120 *
Cavity Radiometer	9.6	9.6	0.12
Total	56.6	61.4	122.5
Total with 15% system margin	**65.1**	**70.7**	**140.9**

*: worst case scenario, assuming no compression is used and individual images are all sent to ground.

3.9 Roadmap

The following developments of critical technology have to be made during Phase 0/A:

For the CR a laboratory prototype has to be built to demonstrate the feasibility of the distributed Electrical Substitution and the characterization of the spatial non uniformity by the sun or by a laser source.

For the WFOV cameras a prototype of the cameras has to be made.

For the spectrometer a prototype of the instruments excluding the calibration sources has to be made, see the details in section 3.4.

For the satellite a detailed design of the solar panel configuration and a mission analysis including a power and thermal analysis has to be made.

3.10 Industrial consortium

The default industrial consortium for the realisation of the Leonardo mission is shown below.

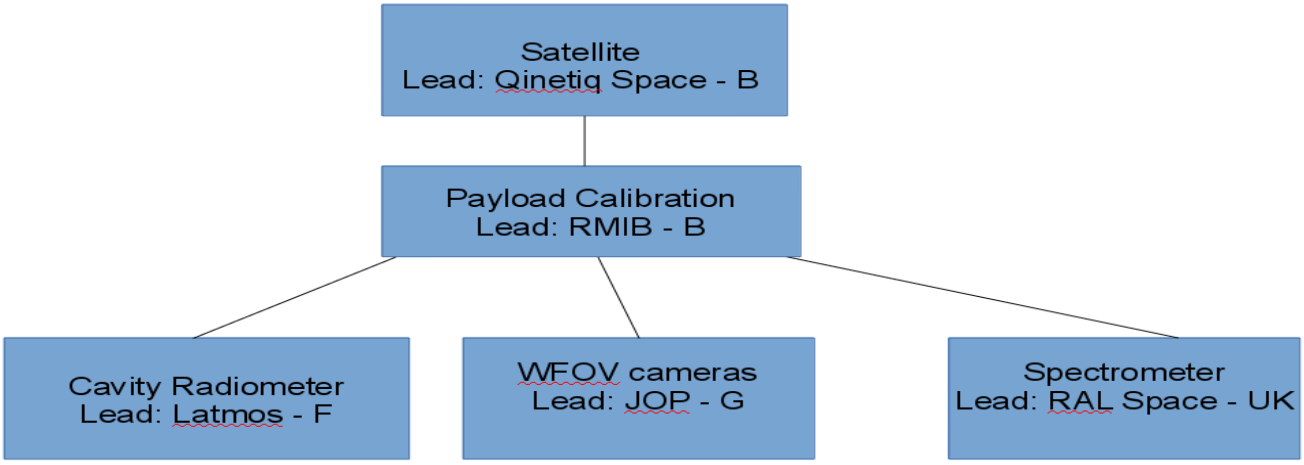

3.11 Cost

The estimated ROM cost for the realisation of the Leonardo mission is given in the table below.

	Cost (Meuro)
Satellite	36.9
Payload Calibration	9.7
Cavity Radiometer	6.4
WFOV cameras	9.9
Spectrometer	59.3
Total	**122.2**

4. Relevance to evaluation criteria

4.1 Relevance to the ESA research objectives for Earth Observation

The Leonardo proposal adresses the following challenges outlined in [ESA, 2015b]:

Atmosphere

—— Challenge A1: Water vapour, cloud, aerosol and radiation processes and the consequences of their effects on the radiation budget and the hydrological cycle.

This is addressed by the core scientific objective of Leonardo to measure the Earth Energy Imbalance and its underlying parameters.

—— Challenge A2: Interactions between the atmosphere and Earth's surface involving natural and anthropogenic feedback processes for water, energy and atmospheric composition.

This is addressed by the measurements of the Earth Energy Imbalance together with the detailed information that can be derived from the broadband spectrometer.

—— Challenge A3: Changes in atmospheric composition and air quality, including interactions with climate.

Leonardo addresses the interactions of aerosols with climate.

—— Challenge A4: Interactions between changes in large-scale atmospheric circulation and regional weather and climate.

This is addressed by the measurement of the spatial and temporal variability of the ERB terms, in particular of the OLR.

Cryosphere

—— Challenge C1: Regional and seasonal distribution of sea-ice mass and the coupling between sea ice, climate, marine ecosystems and biogeochemical cycling in the ocean.

The extent of sea ice can be derived from the Leonardo broadband spectrometer measurements. The melting of sea ice is one of the sources of uncertainty in the estimate of the EEI from OHC, which will be improved by the direct measurement of the EEI by Leonardo.

—— Challenge C4: Effects of changes in the cryosphere on the global oceanic and atmospheric circulation.

This is addressed by the measurement of the spatial and temporal variability of the ERB terms, in particular of the OLR, in particular in the polar regions.

Land Surface

—— Challenge L2: Interactions and feedbacks between global change drivers and biogeochemical cycles, water cycles, including rivers and lakes, biodiversity, and productivity.

This is addressed by the measurements of the Earth Energy Imbalance together with the detailed information that can be derived from the broadband spectrometer.

Ocean

—— Challenge O4: Physical and biogeochemical air–sea interaction processes on different spatiotemporal scales and their fundamental roles in weather and climate.

This is addressed by the joint measurement of Earth Energy Imbalance together with temperature rise, which allows to disentangle the two key climate change uncertainties of aerosol forcing and ocean mixing.

4.2 Need, usefulness and excellence

The measurement of the Earth Energy Imbalance with an accuracy of 0.1 W/m² is considered imperative [Hansen et al, 2011] [von Schuckmann et al, 2016] for understanding current climate change and for predicting future climate change. Hitherto it seemed not feasable to reach the needed accuracy with direct radiative measurements. Leonardo proposes the breaktrough innovation of an accurate differential sun-earth radiation measurement combined with global spatial sampling and a statistical sampling of the diurnal cycle. The accuracy of the Leonardo mission will be beneficial also beyond the lifetime of Leonardo thanks to the synergy with the CERES ERB monitoring program.

4.3 Uniqueness and complementarity

No other existing or planned space mission has the objective to measure the Earth Energy Imbalance with an accuracy of 0.1 W/m². There is a complimentariy with the indirect EEI estimates from Ocean Heat Content derived from the drifting Argo buoys. The accuracy of the indirect OHC based EEI estimate is estimated to be 0.3 W/m² [Trenberth et al., 2016].

4.4 Degree of innovation and contribution to the advancement of European Earth Observation capabilities

The Leonardo Cavity Radiometer is innovative in its design and accuracy.
The Leonardo spectrometer is innovative in its detector concept, using a blackened uncooled microbolometer array for wide swath broadband spectral measurements, and in its telecope design.

4.5 Feasibility and level of maturity

The Leonardo instruments are all based on existing instrument concepts with delta innovations.

The basic concept of measuring the ERB budget at low spatial resolution with cavity radiometers is quite old. Monitoring instruments that have flown in space are the CR's on Nimbus 6 from 1975 to 1978, Nimbus 7 from 1978 to 1993 [Smith et al., 1977; Jacobowitz & Tighe, 1984; Kyle et al. 1993], ERBS from 1984 to 1999 [Luther et al. 1986; Wong et al. 2006]. The use of VACNT and a Gallium phase change cell are innoivations, that have already been demonstrated on the RAVAN cubesat mission [Swartz et al, 2015]. The near spherical cavity design exists on ground [Kim et al, 2014]. The use of spatially distributed Electrical Substitution and the in-

flight solar characterisation of the spatial non-uniformity are new, but they do not pose fundamental problems, and their feasibility will be investigated on a prototype during phase A.

The WFOV SW camera is essentially a modified star tracker with ample flight heritage. For the LW WFOV camera, a ground based WFOV lense exists [NEOS]. Microbolometer arrays are used as infrared imager in the IASI instrument [Hébert et al, 2004] and are used in the MERTIS instrument on BepiColombo [Hiesinger et al, 2010]. A megapixel array was developed for ESA by [INO & Xenics] and a 1024x768 exists from [ULIS]

For the broadband spectrometer the scan mirror concept is based on AVHRR [Hastings, 1992]. The telescope can be a Korsch telescope originally designed for Spacelab [Korsch, 1977] or an innovative freefrom design similar to [Chrisp et al, 2016] . The blackbody and integrating sphere calibration sources as well as the blackened microbolometer array have heritage from the GERB [Harries et al, 2005] and Earthcare BBR [Caldwell et al, 2017a] instruments. The use of a LVF for a spectrometer is demonstrated in [Emadi et al, 2011].

There exists an ERB scientific user community with a long history and many active instruments currently in space [Dewiite & Clerbaux].

4.6 Timeliness

There is an identified user need for increased accuracy of the ERB measurements [Hansen et al, 2011 [von Schuckmann et al, 2016].

There will be a deterioration in sampling of the ERB diurnal cycle with the end of the Ceres instrument on the Terra satellite planned around 2026 [Loeb, 2016]. Leonardo with its precessing orbit will instead deliver an improved sampling of the diurnal cycle.

4.7 Programmatics

Since the Leonardo instruments are based on delta innovations to existing instrument concepts, the development is relatively low risk, and can go relatively fast.

Currently the global monitoring of the ERB budget relies on the US Ceres program, with currently 4 satellites in space (Terra, Aqua, NPP, NOAA-20) and the Ceres follow-on instrument RBI planned on JPSS-2. If successful, the Leonardo mission will provide a European contribution to the global ERB monitoring. By its improved accuracy it will result in a lasting improvement also after the end of its lifetime.

Possibly Leonardo can be the precursor of an operational European ERB monitoring mission in the morning orbit, which would be complimentary to the Ceres missions in the afternoon orbit.

5. References

[Hansen et al, 2011] J. Hansen, M. Sato, P. Kharecha, K. von Schuckmann, “Earth’s energy imbalance and implications”, 2011, Atmos. Chem. Phys., 11, 13421-13449.

[Dewitte & Clerbaux, 2017] S. Dewitte, N. Clerbaux, “Measurement of the earth radiation budget at the top of the atmosphere - a review”, 2017, Remote Sens., 11, 9, 1143.

[von Schuckmann et al, 2016] K. von Schuckmann, M. Palmer, K. Trenberth, A. Cazenave, D. Chambers, N. Champolion, J. Hansen, S. Josey, N. Loeb, P. Mathieu, B. Meyssignac, M. Wild, « An imperative to monitor earth’s energy imbalance », 2016, Nature Climate Change, 6, 138-144.

[Trenberth et al., 2016] K. Trenberth, J. Fasullo, K. von Schuckmann, L. Cheng, « Insights into Earth’s Energy Imbalance from multiple sources », 2016, J. Clim., 29, 7495-7505.

[Loeb et al, 2009] N. Loeb, B. Wielicki, D. Doelling, G. Smith, D. Keyes, S. Kato, N. Manalo-Smith, T. Wong, « Toward optimal closure of the earth’s top-of-atmosphere radiation budget », 2009, J. Climate, 22, 748-766.

[Allan et al, 2017] R. Allan, C. Liu, N. Loeb, M. Palmer, M. Roberts, D. Smith, P-L Vidale, « Changes in global net radiative imbalance 1985-2012 », 2014, GRL, 5588-5598.

[Lyman & Johnson, 2014] J. Lyman, G. Johnson, « Estimating global ocean heat content changes in the upper 1800 m sine 1950 and the influence of climatology choice », 2014, J. Climate, 27, 1945-1957.

[Dewitte & Nevens, 2016] S. Dewitte, S. Nevens, « The Total Solar Irradiance Climate Data Record », 2016, Astrophysical Journal, 830, 25.

[Meftah et al, 2017] M. Meftah et al, « Solar-Iss : a new reference spectrum based on SOLAR/SOLSPEC observations », 2017, Astronomy and Astrophysics, doi: https://doi.org/10.1051/0004-6361/201731316

[Wielicki et al, 2013] B. Wielicki et al, « Achieving climate change accuracy in orbit », 2013, BAMS, 1520-1539, DOI:10.1175/BAMS-D-12-00149.1

[Fox et al, 2011] N. Fox, A. Kaiser-Weiss, W. Schmutz, K. Thome, D. Young, B. Wielicki, R. Winkler, E. Woolliams, « Accurate radiometry from space : an essential tool for climate studies », 2011, Phil. Trans R. Soc., 369, 4028-4063.

[Loeb et al, 2015] N. Loeb, H. Wang, A. Cheng, S. Kato, J. Fasullo, K. Xu, R. Allan, « Observational contraints on atmospheric and oceanic cross-equatorial heat transports : revisiting the precipitation asymmetry problem in climate models », 2016, Clim. Dyn., 46, 3239.

[Frierson et al, 2013] D. Frierson, Y. Hwang, N. Fuckar, R. Seager, S. Kang, A. Donohoe, E. Maroon, X. Liu, D. Battisti, « Contribution of ocean overturning to tropical rainfall peak in the Northern hemisphere », Nat. Geoscience, 6, 940-944.

[Haywood et al. 2016] J.Haywood, A. Jones, N. Dunstone, S. Milton, M. Veillinga, A. Bodas-Salcedo, M. Hawcroft, B. Kravitz, J. Cole, S; Watanabe, G. Stephens, « The impact of equilibrating hemispheric albedos on tropical performance in the HadGEM2-ES coupled climate model », 2016, GRL, 43, 395-403.

[Stephens et al, 2015]G. Stephens, D. O'Brien, P. Webster, P. Pilewski, S. Kato, J. Li, « The albedo of earth », 2015, 53, 141-163.

[Boucher et al, 2013]Boucher, O., D. Randall, P. Artaxo, C. Bretherton, G. Feingold, P. Forster, V.-M. Kerminen, Y. Kondo, H. Liao, U. Lohmann, P. Rasch ,S.K. Satheesh, S. Sherwood, B. Stevens and X.Y. Zhang, 2013: "Clouds and Aerosols. In: Climate. Change 2013: The Physical Science Basis."

[Rosenfeld et al, 2014] D. Rosenfeld. et al, « Global observations of aerosol-cloud-precipitation-climate interactions », 2014, Reviews of Geophysics, 52, 750-808, doi :10.1002/2013RG00441

[Wild, 2009]M. Wild, « Global dimming and brightening : a review », 2009, JGR, 114, D00D16

[Rotstayn & Lohmann, 2002] L. Rotstayn, U. Lohmann, « Tropical rainfall trends and the indirect aerosol effect », 2002, J. Climate, 2103-2116.

[Brocoli et al 2006]A. Brocoli, K. Dahl, R. Stouffer, « Response of the ITCZ to Northern Hemispheric cooling », 2006, GRL, 33, L01702.

[Chang et al 2011]C. Chang, C. Chiang, M. Wehner, A. Friedman, R. Ruedy, « Sulfate aerosol control of tropical atlantic climate over the twentieth century », 2011, J. Climate, 24, 2540-2555

[Bollasino et al, 2011] M. Bollasina, Y. Ming, V. Rawaswamy, « Anthropôgenic aerosols and the weakening of the South Asian summer monsoon », 2011, Science, 334, 502-505.

[Booth et al, 2012] B. Booth, N. Dunstone, P. Halloran, T. Andrews, N. Bellouin, « Aerosols implicated as a prime driver of twentieth-century North Atlantic climate variability », 2012, Nature, 484, 228-232

[Hwang et al 2013]Y. Hwang, D. Frierson, S. Kang, « Anthropogenic sulfate aerosol and the southward shift of tropical precipitation in the late 20th century. », 2013, GRL, 40, 1-6, doi:10.1002/grl.50502.

[Chung & Soden, 2017] E.-S. Chung, B. Soden, « Hemispheric climate shifts driven by anthropogenic aerosol-cloud interactions », 2017, Nat. Geoscience, 10, 566-571.

[Mischenko, 2010] Mishchenko, M.I., 2010: « Review of Satellite Aerosol Remote Sensing Over Land », edited by A.A. Kokhanovsky and G. de Leeuw. J. Quant. Spectrosc. Radiat. Transfer, **111**, 259, doi:10.1016/j.jqsrt.2009.07.011.

[Hong et al, 2016] Q. Hong, Q. Jin, Z. Peng, Z. Yan, H. Liqin, « The introduction of earth radiation measurements on Chinese FY-3 series satellites », ERB workshop, ECMWF, October 2016.

[ESA,2015] ESA, « Science Readyness Level handbook », 2015.

[Harries et al, 2005] J. Harries et al, "The Geostationary Earth Radiation Budget project", 2005, BAMS, 86, 945-960.

[Illingworth et al, 2015] A. Illingworth et al, "The Earthcare satellite. The next step forward in global measurements of clouds, aerosols, precipitation, and radiation", 2015, BAMS,1311-1332, doi:10.1175/BAMS-D-12-00227.1.

[Wielicki et al, 1996] B. Wielicki, B. Barkstrom, E. Harrison, R. Lee, G. Smith, J. Cooper, "Clouds and the Earth's radiant Energy System (CERES): An earth observing experiment", 1996, BAMS, 77, 853-868.

[Minnis et al, 2011] P. Minnis et al, “Ceres Edition-2 cloud property retrievals using TRMM VIRS and Terra and Aqua MODIS data – part 1: Algorithms”,2011, IEEE TGARS, 49 11, 4374-4400.

[Platnick et al, 2015] S. Platnick et al, “MODIS cloud optical propêrties: user guide for the Collection 6 Level-2 MOD06/MYD06 product and associated level-3 datasets”, 2015.

[Sayer et al, 2014] Sayer, A. M., Munchak, L. A., Hsu, N. C., Levy, R. C., Bettenhausen, C., & Jeong, M. J.. (2014). « MODIS Collection 6 aerosol products: Comparison between Aqua's e-Deep Blue, Dark Target, and “merged” data sets, and usage recommendations ».2014, Journal Of Geophysical Research-Atmospheres,. doi:10.1002/2014JD022453

[Rutan et al, 2015] D. Rutan, S. Kato, D. Doelling, F. Rose, L. Nguyen, T. Caldwell, N. Loeb, « CERES synoptic product : methodology and validation of surface radiant flux », 2015, J. Atm. Oc. Tech., 32, 1121-1143.

[Dewitte et al, 2004] S. Dewitte, D. Crommelynck, A. Joukoff, « Total Solar Irradiance observations from DIARAD/.VIRGO », JGR, 109, A02102

[Mekaoui et al, 2010] S. Mekaoui, S. Dewitte, C. Conscience, A. Chevalier, « Total Solar Irradiance absolute level from DIARAD:SOVIM on the International Space Station », 2010, ASR, 45, 1393-1406.

[Dewitte et al, 2012] S. Dewitte, E. Janssen, S. Mekaoui, « Science results from the Sova-Picard Total Solar Irradiance instrument », 2012, AIP Conf. Proc., 1531, 624.

[Meftah et al, 2014] M. Meftah, S. Dewitte, A. Irbah, A. Chevalier, C. Conscience, D. Crommelynck, E. Janssen, S. Mekaoui, 2014, « SOVAP/PICARD, a spaceborne radiometer to measure Total Solar Irradiance », Solar Physics, Vol. 289, pp. 1885-1899, doi:10.1007/s11207-013-0443-0.

[Wong et al, 2006] T. Wong, B. Wielicki, R. Lee, G. Smith, K. Bush, J. Willis, « Reexamination of the observed variability of the Earth Radiation Budget using altitud-corrected ERBE:ERBS nonscanner WFOV data », 2006, J. Clim., 19, 4028-4040.

[Dewitte et al, 2008] S. Dewitte, L. Gonzalez, N. Clerbaux, A. Ipe, C. Bertrand, “The Geostationary Earth Radiation Budget Edition 1 data processing algorithms”, 2008, ASR, 41, 1906-1913.

[Caldwell et al, 2017a], M. Caldwell, D. Spilling, J. Delderfield, K. Ward, M. Whalley, “Radiometric characteristics of the Broad Band Radiometer instrument for EarthCARE space mission”, 2017, J. Atmos. Oceanic Technology, 34, 8, 1783-1794.

[Caldwell et al, 2017b], M. Caldwell et al, “The EarthCARE mission BBR instrument: ground testing of radiometric performance”. 2017, Proc. SPIE, 10402 .

[Karlsson et al, 2012] K-G Karlsson et al, “CLARA-A1: CM SAF cLouds, Albedo and Radiation dataset from AVHRR data - Edition 1 - Monthly Means / Daily Means / Pentad Means / Monthly Histograms”, 2012, doi: 10.5676/EUM_SAF_CM/CLARA_AVHRR/V001.

[Liuzzi et al, 2016] G. Liuzzi, G. Masiello, C. Serio, S. Venafra, C. Camy-Peyret, “Physical inversion of the full IASI spectra: Assessment of atmospheric parameters retrievals, consistency of spectroscopy and forward modelling”. JOURNAL OF QUANTITATIVE SPECTROSCOPY & RADIATIVE TRANSFER, Vol. 182, 128-157, 2016

[Masiello et al, 2015] G. Masiello, C. Serio, S. Venafra, G. Liuzzi, F. Göttsche, I. Trigo, P. Watts, "Kalman filter physical retrieval of surface emissivity and temperature from SEVIRI infrared channels: a validation and inter-comparison study". ATMOSPHERIC MEASUREMENT TECHNIQUES, Vol. 8, 2981-2997, 2015.

[Kim et al, 2014] G. J. Kim, Y. Yoo, B. H. Kim; S. D. Lim, J. H. Song, "A small-size transfer blackbody for calibration of infrared ear thermometers", 2014, Phys. Meas., 35(5):753-62. doi: 10.1088/0967-3334/35/5/753.

[Swartz et al, 2015] W. Swartz, L. Dyrud, S. Lorentz, D. Wu, W. Wiscombe, S. Papadakis, P. Huang, E. Reynolds, A. Smith, D. Deglau, "The RAVAN cubesat mission: progress toward a new measurement of Earth outgoing radiation", 2015, Sun-Climate Symposium, Savannah.

[Hiesinger et al, 2010] H. Hiesinger, J. Helbert, MERTIS CoI Team, "The Mercury Radiometer and Thermal Infrared Spectrometer (MERTIS) for the BepiColombo mission", 2010, Planetary and Space Science, 58, 144-165.

[Korsch, 1977] D. Korsch, "Anastigmatic three-mirror telescope", 1977, Appl. Opt., 16, 8, 2074-2077.

[Chrisp et al, 2016] M. Chrisp, B. Primeau, M. Echter, "Imaging freeform optical systems designed with NURBS surfaces", 2016, Opt. Eng., 55(7), 071208, doi: 10.1117/1.OE.55.7.071208

[ESA,2015b] "ESA'S Living Planet Programme scientific achievements and future challenges", 2015.

[Smith et al. 1977] W. Smith, J. Hickey, H. Howell, H. Jacobowitz, D. Hilleary,, A. Drummond, 1977, "Nimbus-6 Earth Radiation Budget experiment", Appl. Opt., 16, 2, 306-318.

[Jacobowitz & Tighe, 1984] H. Jacobowitz, R. Tighe, "The Earth Radiation Budget data derived from the Nimbus 7 ERB experiment", JGR, 80, D4, 4997-5010.

[Kyle et al. 1993] H. Kyle, J. Hickey, P. Ardanuy, H. Jacobowitz, A. Arking, G. Campbell, F. House, R. Maschhoff, G. Smith, L. Stowe, T. Vonder Haar, "The Nimbus Earth Radiation Budget (ERB) experiment: 1975 to 1992", 1993, BAMS, 815-830.

[Luther et al. 1986] M. Luther., J. Cooper, G. Taylor, 1986: "The Earth Radiation Budget Experiment Nonscanner Instrument", Reviews of Geophysics, 24, 2, 391-399

[NEOS] New England Optical Systems, http://www.neos-inc.com/neos-fisheye-lenses.html

[Hébert et al, 2004] P; Hébert, D. Blumstein, C. Buil, T. Carlier, G. Chalon, P. Astruc, A. Clauss, D. Siméoni, B. Tournier, "IASI instrument: technical descirption and measured perfromances", ESA SP-554, 49–56, 2004.

[INO & Xenics]
http://www.esa.int/Our_Activities/Space_Engineering_Technology/Shaping_the_Future/Vanadium_Dioxide_High_Resolution_Uncooled_Bolometer_Array

[ULIS] https://www.ulis-ir.com/products/pico1024.html

[Hastings, 1992] D. Hastings, "The Advanced Very High Resolution Radiometer (AVHRR): a brief reference guide", 1992, Photogrammetric Engineering and Remote Sensing, 58, 8, 1183-1188.

[Emadi et al, 2011] A. Emadi, H. Wu, G. de Graaf, R. Wolffenbuttel, "IR microspectrometers based on Linear-Variable Optical Filters", 2011, Procedia Engineering, 25, 1401-1404.

[Loeb, 2016] N. Loeb, “State of Ceres”, 2016, ERB workshop, ECMWF.

6. List of acronyms

AOD	Aerosol Optical Depth
AVHRR	Advanced Very High Resolution Radiometer
BB	BlackBody
BBR	BroadBand Radiometer
BPHOT	Brussels Photonic Team
Brb	Broadband
BSM	Back Surface Mirror
CERES	Clouds and the Earth’s Radiant Energy System
CoI	Co-Investigator
CCD	Charge Coupled Device
CMSAF	Climate Monitoring Satellite Application Facility
CNRS	Centre National de Recherche Scientifique
CR	Cavity Radiometer
DM	Development Model
EBAF	Energy Balanced And Filled
EEI	Earth Energy Imbalance
EOL	End Of Life
ERB	Earth Radiation Budget
ERBE	Earth Radiation Budget Experiment
ERBS	Earth Radiation Budget Satellite
ES	Electrical Substitution
ESA	European Space Agency
FOV	Field Of View
FPA	Focal Plane Array
FY	Feng Yung (Chinese meteorological satellite series)
GERB	Geostationary Earth Radiation Budget
GHG	Greenhouse Gas
GSD	Ground Sampling Distance
IASI	Infrared Atmospheric Sounding Interferometer
INO	Institut National d’Optique
IS	Integrating Sphere
JOP	Jena Optronik
JPSS	Joint Polar Satellite System
KNMI	Knoninklijk Nederlands Meteorologisch Instituut
LATMOS	Laboratoire Atmosphères, Milieux, Observations Spatiales
LEONARDO	Low Earth Orbit Novel Advanced Radiation Diurnal Observation
LVF	Linear Variable Filter
LMD	Laboratoire de Météorologie Dynamique
LTAN	Local Time of Ascending Node
LTDN	Lcoal Time of Descending Node
LW	LongWave
MERTIS	Mercury Radiometer and Thermal Infrared Spectrometer
MODIS	Moderate Resolution Imaging Spectrometer

MTH	Mid Tropospheric Humidity
NEOS	New England Optical Systems
NIR	Near InfraRed
NPP	NPOES Preparatory Program
NOAA	National Oceanographic and Atmospheric Agency
OHC	Ocean Heat Content
OLR	Outgoing Longwave Radiation
PI	Principal Investigator
P/L	Payload
PLF	Payload Face
QS	QinetiQ Space
RAL	Rutherford Appleton Laboratory
RAVAN	Radiometer Assessment using Vertically Aligned Nanotubes
RBI	Radiation Budget Instrument
RMIB	Royal Meteorological Institute of Belgium
ROIC	Readout Electronics
RSR	Reflected Solar Radiation
SEVIRI	Spinning Enahanced Visible and Infrared Imager
SG	Second Generation
SNS	Surrey NanoSystems
SNR	Signal to Noise Ratio
SRL	Scientific Readiness Level
SSO	Sun Synchronous Orbit
SW	ShortWave
SYN	Synoptic
TOA	Top Of Atmosphere
TRL	Technical Readiness Level
TSI	Total Solar Irradiance
US	United States
UTH	Upper Tropospheric Humidity
UV	UltraViolet
VACNT	Vacuum Aligned Carbon NanoTubes
VIS	Visible
VUB	Vrije Universiteit Brussel
WFOV	Wide Field Of View
WV	Water Vapour